# Provenance and recycling of Sahara Desert sand

Guido Pastore[1], Thomas Baird[2], Pieter Vermeesch[2], Alberto Resentini[1], Eduardo Garzanti[1*]

[1]*Laboratory for Provenance Studies, Department of Earth and Environmental Sciences, University of Milano-Bicocca, 20126 Milano, Italy*

[2] *London Geochronology Centre, Department of Earth Sciences, University College London, London, WC1E 6BT, UK*

Email: g.pastore2@campus.unimib.it (Pastore), thomas.baird.16@ucl.ac.uk (Baird), p.vermeesch@ucl.ac.uk (Vermeesch), alberto.resentini@unimib.it (Resentini), eduardo.garzanti@unimib.it (Garzanti),

* Corresponding author

*Key words*: Sand petrography; Heavy minerals; U-Pb zircon ages; Multivariate statistics; Sedimentary processes; Recycling; Fluvial/eolian interactions; Wind-fed and river-fed sand seas; Pan-African Orogeny.

## ABSTRACT

We here present the first comprehensive provenance study of the Sahara Desert using a combination of multiple provenance proxies and state-of-the-art statistical analysis. Our dataset comprises 44 aeolian-dune samples, collected across the region from 12°N (Nigeria) to 34°N (Tunisia) and from 33°E (Egypt) to 16°W (Mauritania) and characterised by bulk-petrography, heavy-mineral, and detrital-zircon U–Pb geochronology analyses. A set of statistical tools including Multidimensional Scaling, Correspondence Analysis, Individual Difference Scaling, and General Procrustes Analysis was applied to discriminate among sample groups with the purpose to reveal meaningful compositional patterns and infer sediment transport pathways on a geological scale. The overall homogenity across sand samples, however, precluded a detailed narrative.

Saharan dune fields are, with a few local exceptions, composed of pure quartzose sand with very poor heavy-mineral suites dominated by durable zircon, tourmaline, and rutile. Some feldspars, amphibole, epidote, garnet, or staurolite occur closer to basement exposures, and carbonate grains, clinopyroxene and olivine near a basaltic field in Libya. Relatively varied compositions also characterize sand along the Nile Valley and the southern front of the Anti-Atlas fold belt in Morocco. Otherwise, from the Sahel to the Mediterranean Sea and from the Nile River to the Atlantic Ocean, sand consists nearly exclusively of quartz and durable minerals. These have been concentrated through multiple cycles of erosion, deposition, and diagenesis of Phanerozoic siliciclastic rocks during the long period of relative tectonic quiescence that followed the Neoproterozoic Pan-African orogeny, the last episode of major crustal growth in the region. The principal ultimate source of recycled sand is held to be represented by the thick blanket of quartz-rich sandstones that were deposited in the Cambro-Ordovician from the newly formed Arabian-Nubian Shield in the east to Mauritania in the west. Durability of zircon grains and their likelihood to be recycled from older sedimentary rocks argues against the assumption, too often implicitly taken for granted in provenance studies based on detrital-zircon ages, that their age distribution reflects transport pathways existing at the time of deposition rather than inheritance from multiple and remote landscapes of the past.

"*I have always loved the desert. You sit down on a sand dune. You see nothing. You hear nothing. And yet something shines, something sings in that silence*."
Antoine de Saint-Exupéry, The Little Prince

## 1. Introduction

The Sahara is by far the largest hot desert on Earth, hosting several large dune fields. The provenance of these vast expanses of sand is gravely understudied. We here present the first thorough and comprehensive multisdisciplinary study aimed at understanding the nature of sand sources, how sand evolved during geological time, and under the action of which prevailing wind regimes and along which trajectories was it displaced and eventually accumulated in the sand sea.

Our main purpose is to contribute to the ongoing debate in sedimentology and in Quaternary paleoclimatology concerning the production of sand and silt in arid landscapes. As far as quartzose sand is concerned (Dott, 2003; Muhs, 2004), one view is that sediment delivered from surrounding source rocks "matures" by essentially mechanical processes within the desert area (e.g., Dutta et al., 1993). Another is that the concentration of durable minerals is inherited from recycling of older sandstones that underwent extensive weathering in more aggressive climatic conditions, extensive intrastratal dissolution during diagenesis, or in general multiphase chemical leaching during multiple cycles of weathering and diagenesis (e.g., Garzanti, 2017).

Even more controversial are the generation mechanisms of "desert loess" (Smith et al., 2002; Lancaster, 2020). Throughout the Plio-Quaternary, the Sahara has represented a major source of fine particles, blown offshore to as far as the other side of the Atlantic Ocean (Muhs et al., 1990, 2019; Prospero, 1996) and is currently the largest source of mineral aerosols globally (Tegen et al., 2013). Up to 85 megatonnes of dust are emitted into the atmosphere from the Sahara annually, with the Bodélé Depression representing the largest single area of dust production (Middleton and Goudie, 2001; Koren et al., 2006; Bakker et al., 2019). However, the precise mechanism behind the origin of mineral aerosol is hotly debated. Studies have suggested the predominant genesis for dust emissions is the deflation of fine-grained sediments from depressed areas (e.g., Bristow et al., 2009), the abrasion of saltating sand grains within sand seas (e.g., Crouvi et al., 2012), or the accumulation of silt through hydrological factors, resulting in high emissions from alluvial deposits, desiccated lake beds, and palaeolakes (Bakker et al., 2019; Jewell et al., 2020). The need to identify major sediment sources and clarify the process of sand and silt generation through tracing the main directions of aeolian transport within the Sahara are therefore much warranted.

This study investigates the origin, spatial variability, and transport pathways of aeolian sand in the Sahara by combining bulk-petrography, heavy-mineral, and detrital-zircon U–Pb geochronology analyses on 44 sediment samples. These samples have been collected in northern Africa across more than 20° degrees of latitude from the Sahel to the Mediterranean Sea and almost 50° degrees of longitude from the Nile River to the Atlantic Ocean (Fig. 1).

Highly detailed provenance studies of desert sand have been carried out with the same multitechnique approach in diverse sand seas of Africa, Arabia, and Asia (e.g., Garzanti et al., 2012, 2017; Stevens et al., 2013; Rittner et al., 2016) but not on the Sahara so far. Saharan dune sands have been broadly described as composed of quartz (e.g., El-Baz, 1998; Muhs, 2004; Abdelhak et al., 2014; Meftah and Mahboub, 2020) but their provenance has remained unknown. To identify the source regions, gain understanding of sand transport pathways, and extract all possible provenance information from a composition characterized by only a limited number of provenance-diagnostic minerals, our study required the scrutiny of multi-proxy datasets using a full set of advanced statistical techniques. Multidimensional Scaling, Correspondence Analysis, Individual Difference Scaling, and General Procrustes Analysis were applied to provide both a highly robust statistical investigation and an unbiased visual representation of the relationships among the samples.

## 2. Geomorphological framework

### *2.1. Climate and wind patterns*

The Sahara (in Arabic *sahra*, desert) covers an area of 9 million $km^2$ and extends from ~12°N to ~34°N (Fig. 1). The desert thus straddles the Tropic of Cancer and is influenced by the descending limb of the Hadley cell. The trajectory of air masses and rainfall are regulated by the strength of the subtropical high-pressure system and by the latitudinal shift of the Intertropical Convergence Zone (ITCZ). Average annual precipitation is <50 mm in most areas, which may not see rain in many consecutive years, and increases to ~160 mm in the semiarid Sahel to the south (from either the Arabic word *sahil*, shore, figurative for desert's edge, or *sahl*, plain).

During winter, the ITCZ shifts to the south and the Azores Anticyclone and the Sahara High are established, with only occasional disturbances by cyclonic systems from the Atlantic Ocean or by the polar front. Atmospheric circulation is dominated by westerly winds and by winds associated with the Mediterranean depression, and the only maritime air masses enter the Sahara from the Red Sea. In the spring, the *khamseen* wind (in Arabic *khamseen*, fifty, because the wind blows over ~50 days) moves hot tropical air towards the Mediterranean coast. In the summer, the northward displacement of the ITCZ allows air masses blown by recurved south-easterly trade winds to penetrate the continent, and the West African Monsoon brings moisture to the southern Sahara. In its northern position, the ITCZ represents a barrier for air masses blown by the hot and dry north-easterly trade winds (the *harmattan;* possibly derived indirectly from the Arabic word *haram*, evil), often regulated daily by the thermic inversion of near-surface air (Warner, 2009). Libya reaches one of the highest temperatures on Earth (58°C) with extreme diurnal variation (up to 50°C), whereas lower temperatures are recorded in the northwest influenced by the incursion of cold air from the Atlantic Ocean.

A climatic zonation distinguishes the northern Sahara, affected by the winter Mediterranean depression, and the southern Sahara, characterized by the West African Monsoon in summer. This zonation is strengthened by the position of the main topographic highs (Hoggar, Tibesti, and Ennedi Mountains), hampering precipitations and southward sand transport from north to south (Wilson, 1971; Mainguet, 1978). Relief concentrates precipitation in summer and extreme events and flash floods occur when the monsoon pushes humid air against the Tibesti and Hoggar massifs.

Saharan sand-flow patterns are poorly constrained. Historically, the role of the subtropical high-pressure zone has been argued to split sand flows along a north-south divide (Wilson, 1971). In the northern zone, transport occurs mainly to the northeast, while the southern zone sees sand flow towards the coast of Mauritania and offshore into the Atlantic Ocean (Fig. 2). However, this theory relies on a short temporal sampling window and warrants revisiting.

## *2.2. Hydrology*

Because of extreme aridity, river courses in the Sahara are transformed into desiccated dry valleys (in Arabic *wadi*, plural *widyan*), representing the remnants of the hydrological network inherited from wetter climatic stages in the past (Ghoneim et al., 2007; Abdelkareem and El-Baz, 2015; Abdelsalam, 2018). One example in the eastern Sahara is Wadi Howar (Fig. 1), sourced from the Ennedi and Darfur mountains and once draining northeastwards from the Chad/Sudan border to the Nile for 640 km but now marked only by linear tree vegetation sustained by the groundwater table in the shallow subsurface (Pachur and Kröpelin, 1987). The major exception is the Nile River (basin area ~3 million km$^2$), which conveys across the desert the large volume of water received from East African lakes, augmented by monsoonal rains falling on the Ethiopian plateau in the summer (Sutcliffe and Parks, 1999).

The southeastern Sahara Desert receives water from the laterite-capped hilly plateau representing the water divide from the Congo and the source of several headwater branches of the Bahr El Ghazal, a western tributary of the Nile (in Arabic *bahr*, sea, figurative for big river). To the west, the Chari River and its major western Logone branch drain the Cameroon basaltic plateau to feed Lake Chad, a shallow body of water (depth mainly < 7 m) surrounded by seasonally inundated marshland (Fig. 1). Lake Chad is the only lake remaining in the desert, with a vast (2.5 million km$^2$) endorheic drainage basin that receives monsoonal rain falling during summer in the south. Climate change and increased water use for human activities make the lake vulnerable to drought events such as those of the 1970s and 1980s, which saw the lake surface area shrink by up to 90% (Birkett, 2000; Coe and Foley, 2001; Gao et al., 2011).

Farther west, the Niger River (basin area 2.3 million km$^2$), sourced in the Guinea plateau only ~250 km from the Atlantic coast, draws a wide arc across the southern Sahara passing through an inland delta in Mali and is eventually diverted southward towards the Gulf of Guinea (Gischler, 1976; Goudie, 2005). The Atlas Mountains collect precipitation also in the form of snow, recharging the large aquifers of the northwestern Sahara (Al-Gamal, 2011). In the eastern Sahara, subsurface water is stored in Nubian sandstone acquifers across the political borders of Libya, Egypt, Sudan, and Chad (Gossel et al., 2004).

### *2.3. Sand dunes*

Sand dunes cover only a fifth of the immense surface of the Sahara. In order to understand the relationships with wind regimes, dune forms and distribution have long been studied with field expeditions (e.g., Bagnold, 1942; Capot-Rey, 1945) and satellite images (Breed et al., 1979; Lancaster, 1995; El-Baz, 2000; Pye and Tsoar, 2008; Baird et al., 2019). Mainguet and Chemin (1983) suggested that the central part of the desert, which is subjected to strong deflation, represents a major source of sand for dune fields along its margins, where more humid climate, vegetation, and decreased wind strength induce deposition especially close to the main topographic barriers.

In the western Sahara, linear dunes predominate from the coast inland, whereas crescentic dunes are common to the south, associated with north-easterly anticyclonic circulation from the Sahara and Azores high-pressure cells. In Mali and Niger, most dunes are partially vegetated under the influence of monsoonal moisture. Two sets of dunes occur along the Niger River, one indicating northeastward drift induced by trade winds, and the other oriented E/W with more spaced and eroded ridges. Crescentic dunes and large isolated star dunes characterize the Erg de Bilma in Niger (Fig. 1; Mainguet and Callot, 1978).

In the Moroccan desert close to the Atlantic coast, barchan dunes form under the effect of prevailing winds from the northwest and moderate to low sand supply (Elbelrhiti, 2012). In the northern Sahara, large sand seas with star dunes occupy depressions bordered by elevated areas. Star dunes are the product of a complex, multi-directional wind regime (Lancaster, 1995; Zhang et al., 2012), resulting from the interaction of winter westerlies with summer north-easterly and south-westerly winds generated from cyclonic perturbations in Mediterrean and Atlantic depression systems. Star dunes occur in the northern part of the Grand Erg Occidental, grading southward into crescentic dunes, and are aligned in linear trends in the Grand Erg Oriental. A network of barchanoid dunes in southern Tunisia is generated by high-energy winds, whereas crescentic or linear dunes grown in response to unimodal or bimodal wind directions are more common south of 30°N (Breed et al., 1979).

*2.4. Quaternary evolution*

Dry and wet climate alternated repeatedly in northern Africa during the Quaternary. Wind strength fostering dune growth increased in the latest Pleistocene, followed by a humid early Holocene and eventually by the return to arid conditions since the mid-Holocene. The desert expanded during the Last Glacial Maximum, when the ITCZ was displaced towards the equator (Nicholson and Flohn, 1980; Arbuszewski et al. 2013) and dunes mobilized by stronger wind moved onto arid landscapes (Grove and Warren, 1968; Swezey, 2001; Bristow and Armitage, 2016). Arid to humid transitions seemingly occurred at 15-14.5 ka and 11.5-11 ka, in association with the reduction of polar ice-sheets, strengthened hydrological circulation (Gasse, 2000), and northward displacement of the ITCZ (Haug et al., 2001).

At the onset of the early Holocene African Humid Period (~14.5 ka), natural corridors opened to allow the displacement of humans and other animals (Kuper and Kropelin, 2006; Drake et al., 2011). The current aridity initiated between ~5.5 ka (deMenocal et al., 2000) and ~4.5 ka (Gasse, 2000), but the timing and rate of desiccation that affected the Sahara and Sahel at the end of the African Humid

Period, including Mega-Lake Chad, remain controversial (Sarnthein, 1978; Bristow and Armitage, 2016).

## 3. Geological framework

Four partially overlapping geological domains can be identified in the Sahara Desert (Fig. 3): 1) the West African Craton, representing the oldest core of the continent; 2) the Tuareg Shield, including different sub-domains from east to west; 3) the Sahara Metacraton in the east, where the Archean cratonic core was intensely remobilized during the Pan-African orogeny; 4) Phanerozoic cover strata in the northern part of the desert, accumulated during multistep episodes of basin subsidence, tectonic inversion, and volcanic activity.

### *3.1. West African Craton*

The West African Craton comprises the Man Shield in the south and the Reguibat Shield in the north. These terranes include an Archean core, built during the Leonian (3.0-2.9 Ga) and Liberian (2.7-2.6 Ga) orogenic cycles (Feybesse and Milési, 1994), bordered by Proterozoic to Phanerozoic mobile belts and sedimentary basins. The eastern Reguibat Shield and the Man Shield were affected by the Eburnean orogeny (~2.0 Ga), when the high-grade Birimian basement formed (Abouchami et al., 1990). The Anti-Atlas Mountains in Morocco also contain Paleoproterozoic basement, including granites as well as metasedimentary and metavolcanic rocks (Thomas et al., 2002).

During the Pan-African orogeny (0.85-0.55 Ga), one of the most extensive mountain-building events of the Earth's history that assembled the Arabian-Nubian Shield and deeply affected the Sahara Metacraton, the 3000 km-long Trans-Sahara belt formed as a result of collisions among the West African Craton, the Congo Craton, and the Sahara Metacraton. High sediment influx caused the filling of the Taoudeni (in the south) and Tindouf (in the north) intraplate basins (Fig. 3; Nance et al., 2008). Low-grade metamorphism and granite intrusions took place along the margins of the West African Craton (Black et al., 1979), whereas volcanic sequences and transpressional deformation are documented in the Anti-Altas to the north (Ennih and Liégeois, 2001). In the east, the Pan-African event is responsible for the formation of thrust belts along the western side of the West Africa Craton (Villeneuve, 2008), which developed only minor tectonic structures in the foreland of the Paleozoic Variscan orogeny (Ennih and Liégeois, 2008). The Cenozoic Alpine orogeny affected only the northernmost part of the African continent forming the High Atlas of Morocco (Mattauer et al., 1977).

*3.2. Tuareg Shield*

The Tuareg Shield, located between the West African Craton in the west and the Sahara Metacraton in the east, developed during the Neoproterozoic by eastward subduction and closure of the Aoujej and Imira oceanic realms at 700 and 625 Ma, and consequent accretion of different terranes (Caby et al. 1981, 1989; Fabre et al., 1982). High-temperature N/S shear zones were interpreted to document post-collisional lateral escape of rigid tectonic blocks (Liégeois, 2019).

During the Pan-African orogeny, granulitic gneisses of Archean and Paleoproterozoic age in the central Hoggar (e.g., Unitè Granulitique de Iforas) were remobilized with development of amphibolite-facies mega-shear zones (Liégeois et al., 1994) and the Tuareg Shield was heavily reworked (Bertrand and Caby, 1978). To the southwest, the Adrar des Iforas Massif recorded several magmatic events, including emplacement of the Renatt leucogranite (Liégeois et al., 1994), continental-arc andesites (Chikhaoui et al., 1978), alkaline plutons between 600 and 580 Ma (Fezaa et al., 2019), as well as late/post orogenic plutons, dykes, and volcanic rocks between 570 and 520 Ma (Liégeois and Black, 1987).

The Aïr Mountains in the southwestern Tuareg Shield include three N/S elongated terranes (Aouzegueur, Barghot, and Assodé) containing high-grade metasedimentary rocks and serpentinites (Boullier et al., 1991; Moreau et al., 1994). Granites cross-cutting the main deformation were intruded at 664±8 Ma in the Barghot domain and between 645 and 580 Ma in the Assodé domain (Liégeois et al., 1994). The Aouzegueur and Barghot terranes were thrust eastward over the Saharan Metacraton in the late Neoproterozoic (Liégeois et al., 2000). A ring complex including anorthosite was emplaced in the Aïr Mountains during the early Devonian (Black, 1965), whereas Cenozoic magmatism was volumetrically negligible.

The northeastern border of the Tuareg Shield was affected by a major intracontinental tectono-magmatic event at 575–555 Ma, associated with the indentation of the cratonic basement of the Murzuq Basin (Fezaa et al., 2010).

### 3.3. *Sahara Metacraton*

The Saharan Metacraton (Fig. 3), separated by a mega-shear from the Tuareg Shield in the west and from the Arabian-Nubian Shield in the east, consists of Archean and Paleoproterozoic continental crust profoundly remobilized during the Pan-African orogeny, when migmatitic gneisses and metasedimentary rocks were intruded by granitoids between 750 and 550 Ma (Abdelsalam et al., 2002). Various geodynamic processes, including continental collision (Schandelmeier et al., 1988), delamination of subcontinental mantle (Bird, 1979), lithospheric extension (Denkler et al., 1994), and assemblage of exotic terranes (Rogers et al., 1978) have been invoked to explain the Neoproterozoic evolution of the metacraton (Ghuma and Rogers, 1978; Pinna et al., 1994). In the east, an ophiolitic suture contains low-grade volcaniclastic rocks possibly documenting the closure of a failed rift (Stern et al., 1994; Kuster and Liegeois, 2001).

### *3.4. Phanerozoic sedimentary and volcanic rocks*

The northern part of the Sahara is largely covered by Paleozoic to Cenozoic rocks deposited in sedimentary basins formed in the wake of the Pan-African orogeny and subsequently by extensional reactivation of inherited tectonic structures (Echikh, 1998; Bumby and Giraud, 2005).

Between the mid-Cambrian and the Late Ordovician (520-440 Ma), quartz-rich sandstones where deposited all across northern Africa, possibly as a continuous blanket from Oman in eastern Arabia to Mauritania with an average thickness of ~1 km and a volume of ~10 million km$^3$ (Burke, 1999). Their deposition followed the Pan-African orogeny and post-Pan-African continental wrenching, and characterized the ensuing phase of cooling and thermal subsidence that generated the accommodation space for the widespread accumulation of sand sheets. At that time, quartz-rich sandstones were deposited also in other parts of Gondwana and even in North America (e.g., St. Peter Sandstone; Dott, 2003). Quartz-rich composition is highly unusual for orogenic detritus (Dickinson, 1985; Garzanti et al., 2007), an anomaly that still needs understanding. If these sediments are indeed first cycle, then *ad hoc* explanations are required. Cambro-Ordovician landscapes still devoid of vegetation and supposedly characterized by low relief and low sedimentation rates are envisaged to have suffered very extensive chemical weathering, fostered by warm humid climate and by an unusually corrosive atmosphere following late Neoproterozoic volcanism (Burke, 1999; Avigad et al., 2005). This scenario is apparently at odds with the major glaciation that affected Gondwana in the Late Ordovician, which itself represents a geological paradox, having occurred within a long greenhouse period with high atmospheric $CO_2$ levels (Brenchley et al., 1994; Ghienne et al., 2014).

In the Silurian, tectonic subsidence favoured the accumulation of marine to lacustrine sediments, overlain by shallow-marine clastics in the Murzuq Basin of Libya, in western Algeria, and in southern Morocco (Fekirine and Abdallah, 1998). Failed rifts were inverted during the Carboniferous as a consequence of Variscan convergence, affecting mostly Morocco and less intensely Algeria and Libya (Haddoum et al., 2001). The High Atlas graben system formed in the Triassic and Jurassic extending eastwards to northeastern Algeria and Tunisia (Coward and Ries, 2003). During the Cretaceous, the Sirte Basin developed as another horst-and-graben system filled by shale and evaporite (Thusu and Mansouri, 1995). In the northern Murzuq Basin, these strata are overlain by basaltic lavas of the Haruj al Aswad Massif, emplaced in multiple phases between 4 and 0.5 Ma and triggered by reactivation of Tibesti-Sirte basement faults (Cvetković et al., 2010; Elshaafi and Gudmundsson, 2016).

## 4. Sampling and methods

In this study, we analysed an archive of 45 sand samples of aeolian dunes, 36 collected between 2003 and 2019 by different operators across the Sahara Desert: 4 from Chad; 5 from Lake Chad, northern

Nigeria, and southern Niger; 8 from central Niger; 1 from Burkina Faso; 2 from Mali; 4 from Mauritania; 3 from Morocco; 3 from Algeria; 2 from Tunisia; 3 from Libya; and 1 from western Egypt. Data are also provided for 9 additional aeolian dunes from Egypt: 3 from the Western Desert and 6 from the Nile Valley to the west of the Nile River. Aeolian dunes to the east of the Nile River containing Nile-derived volcanic detritus (Muhs et al., 2013; Garzanti et al., 2015a) were considered as separated from the rest of the Sahara and thus not included in this study. GPS coordinates and further information on all sampling sites are provided in Appendix Table A1 and Google Earth™ file Sahara.kmz.

### *4.1. Petrography*

Bulk sand samples were impregnated with araldite epoxy, cut into standard thin sections, and analysed by counting 450-500 points under the petrographic microscope (Gazzi-Dickinson method; Ingersoll et al., 1984). Sand classification was based on the relative abundance of the three main framework components quartz (Q), feldspars (F), and lithic fragments (L), considered if exceeding 10%QFL. According to standard use, the less abundant component goes first, the more abundant last (e.g., a sand is named litho-quartzose if Q > L > 10%QFL > F). Feldspar-rich feldspatho-quartzose (1 < Q/F < 2), feldspatho-quartzose (2 < Q/F < 4), quartz-rich feldspatho-quartzose (4 < Q/F < 9), quartzose (90% < Q/QFL < 95%), and pure quartzose compositions (Q/QFL > 95%) are distinguished (classification scheme after Garzanti, 2019). These distinctions are essential to discriminate among quartz-rich suites generated in anorogenic settings (Garzanti et al., 2001, 2018a). Metamorphic rock fragments were subdivided into very low to low-rank metasedimentary or metavolcanic, and medium to high-rank felsic or mafic categories (Garzanti and Vezzoli, 2003). The intrabasinal *versus* extrabasinal origin of carbonate and non-carbonate grains was established based on criteria illustrated in Zuffa (1985) and Garzanti (1991). Petrographic parameters used in this article include the plagioclase/total feldspar (P/F) ratio; feldspar identified by cross-hatch twinning is called microcline* through the text. Median grain size was determined in thin section by ranking and visual comparison with in-house standards composed of mounts of sieved Φ/4 classes. Key petrographic parameters are provided in Table 1 and the complete petrographic dataset in Appendix Table A2.

### *4.2. Heavy minerals*

From a split aliquot of each sample of well sorted aeolian sand, the dense fraction was separated by centrifuging in Na-metatungstate (density 2.90 g/cm$^3$) and recovered by partial freezing with liquid nitrogen (method described in detail in Andò, 2020). Samples were analysed in bulk to obtain a faithful characterization of the entire heavy-mineral suite. In order to determine correct volume percentages, ≥ 200 transparent heavy minerals were point-counted at suitable regular spacing on each grain mount (Garzanti and Andò, 2019). In previous analyses of 9 Egyptian samples, different size fractions were used (> 95 or 95-500 µm for Western Desert samples and 63-250 µm for Nile Valley samples) and heavy minerals were counted by the area method (Galehouse, 1971).

Transparent heavy-mineral assemblages, called for brevity "tHM suites" throughout the text, are defined as the spectrum of detrital extrabasinal minerals with density >2.90 g/cm$^3$ identifiable under a transmitted-light microscope. Rock fragments, iron oxides, soil clasts, phyllosilicates, and carbonates were not considered as integral part of the tHM suite. According to the concentration of transparent heavy minerals (tHMC), tHM suites are described as "extremely poor" (tHMC < 0.1), "very poor" (0.1 ≤ tHMC < 0.5), "poor" (0.5 ≤ tHMC < 1), and "moderately poor" (1 ≤ tHMC < 2). The ZTR index (sum of zircon, tourmaline and rutile over total tHM; Hubert 1962) expresses the durability of the tHM suite. Significant detrital components are listed in order of abundance (high to low) throughout the text. Key heavy-mineral parameters are provided in Table 1 and the complete dataset in Appendix Table A3.

### *4.3. Detrital geochronology*

Detrital zircons were identified by Automated Phase Mapping (Vermeesch et al., 2017) with a Renishaw inVia™ Raman microscope on the heavy-mineral separates of 32 selected samples, concentrated with standard magnetic techniques and directly mounted in epoxy resin without any operator selection *via* hand picking. U-Pb zircon ages were determined at the London Geochronology Centre using an Agilent 7900 LA-ICP-MS (laser ablation-inductively coupled plasma-mass spectrometry) system, employing a NewWave NWR193 Excimer Laser operated at 10 Hz with a 25 µm spot size and ~2.5 J/cm$^2$ fluence. No cathodo-luminescence imaging was conducted, and the laser spot was always placed "blindly" in the middle of zircon grains in order to treat all samples equally and avoid bias in intersample comparison ("blind-dating approach", illustrated and discussed in Garzanti et al., 2018b). Many samples were subsequently analysed targeting zircon rims and nearly identical results were obtained. No common Pb correction was applied. The mass spectrometer data were converted to isotopic ratios using GLITTER 4.4.2 software (Griffin et al., 2008), employing Plešovice zircon (Sláma et al., 2008) as a primary age standard and GJ-1 (Jackson et al., 2004) as a secondary age standard. A NIST SRM612 glass was used as a compositional standard for U and Th concentrations. GLITTER files were post-processed in R using IsoplotR 2.5 (Vermeesch, 2018a). We used $^{206}Pb/^{238}U$ and $^{207}Pb/^{206}Pb$ as preferred ages for zircons younger and older than 1100 Ma, respectively. We calculated concordia ages as the maximum likelihood intersection between the concordia line and the error ellipse of $^{207}Pb/^{235}U$ and $^{206}Pb/^{238}U$ ages (Ludwig, 1998; Vermeesch, 2021); ages with >-5/+15% relative discordance were considered discordant. The concordia ages were used for statistical analysis. The complete geochronological dataset, comprising ~4000 concordant ages (> 100 ages on 26 samples) is provided in Appendix B.

### *4.4. Statistical tools*

Multidimensional Scaling (MDS; Kruskal and Wish, 1978; Vermeesch, 2013) is a multivariate ordination technique that takes a dissimilarity matrix as input and produces a map of samples as output, in which similar samples plot close together and dissimilar samples plot far apart. For detrital zircon U-Pb age spectra, a dissimilarity matrix can be constructed using the Kolmogorov-Smirnov statistic (i.e., the maximum vertical difference between two cumulative distribution functions; Feller, 1948). Correspondence Analysis (CA) is an ordination technique that is specifically tailored for count data such as petrographic and heavy-mineral point counts (Greenacre, 2017). This method can be shown to be a special case of MDS in which the dissimilarity matrix is populated with chi-square distances (Vermeesch, 2018b).

General Procrustes Analysis (GPA) and Individual Difference Scaling (INDSCAL) are higher-order data-mining techniques that combine several MDS maps together in order to simplify the interpretation of 'big' datasets (Vermeesch and Garzanti, 2015). In the case of GPA, this is achieved by mapping the different MDS configurations onto a common configuration by a number of affine transformations (reflection, rotation, scaling, and translation; Gower, 1975). INDSCAL, on the other hand, acts directly on the dissimilarity matrices. It is a higher order generalisation of the MDS method that aims to fit multiple dissimilarity matrices to a shared 'group configuration' by attaching different weights to the different datasets (Carroll and Chang, 1970).

Dissimilarity matrices for the different provenance proxies for multivariate ordination were also used to construct hierarchical clustering dendrograms with the normalised distance values obtained by chi-squared distance (for CA) and Kolmogorov-Smirnov distance (for MDS). Thus we were able to assign the samples to different clusters, thereby augmenting further the visual interpretation (Fig. 8A,B,C). The same method was applied to the GPA matrices of dissimilarities displayed in Fig, 8E,F. Additional statistical tools are presented in Appendix C.

To illustrate heavy-mineral data we used the compositional biplot (Gabriel, 1971; Greenacre, 2017), a statistical/graphical display that allows discrimination among multivariate observations (points) while shedding light on the mutual relationships among multiple variables (rays). The length of each ray is proportional to the variance of the corresponding variable in the dataset. If the angle between two rays is close to 0°, 90° or 180°, then the corresponding variables are directly correlated, uncorrelated, or inversely correlated, respectively.

## 5. Results

In this section we shall first summarize the general petrographic, heavy-mineral, and detrital-geochronology signatures of Saharan dune sands. Next, we shall highlight the characteristic compositional features of each region (Fig. 4).

*5.1. Overview of detrital signatures*

Most analysed sand samples (33 out of 44) are pure quartzose (Fig. 5), including all of those from the southeastern Sahara. In pure quartzose sands, orthoclase generally prevails over plagioclase and microcline*. The sum of lithic grains, micas and heavy minerals is <2% of total framework grains. The tHM suites of most samples (35 out of 44) are very poor to extremely poor and characterized by durable minerals (ZTR 25-96, anticorrelating with tHMC: r = 0.62, sign.lev. 0.1%) (Fig. 6). Zircon is most common, followed by tourmaline, epidote, amphibole, rutile, clinopyroxene, garnet, and staurolite.

Detrital zircon in Saharan dunes invariably yielded dominant Pan-African (Ordovician-Neoproterozoic) U-Pb ages, with a virtually continuous distribution between 0.48 and 1.1.Ga (77% of total ages), a prominent Cambrian-Ediacaran peak (0.5-0.6 Ga), a minor peak around 1.0 Ga, and an intervening broader cluster in the Cryogenian (0.65-0.8 Ga) (Fig. 7). Younger ages are Paleozoic (1.6%), Mesozoic (0.5%) and Cenozoic (0.2%). Older ages cluster between 1.8 and 2.2 Ga (11.7%) and between 2.47 and 2.7 Ga (2.8%). Zircon grains dated between 1.1 and 1.8 Ga and between 2.2 and 2.47 Ga represent 3.4% and 1.2% of total ages, respectively, whereas those older than 2.7 Ga represent 1.6%, with single ages as old as ~4 Ga.

*5.2. The southern Sahara*

All across the southern Sahara, from Chad to the Atlantic Ocean, dune sand displays rather monotonous detrital signatures (Table 1). Both around the Bodélé Depression and in the Lake Chad region sand is pure quartzose with high ZTR indices (Fig. 4F, 4I). Minor K-feldspar occurs (sample

5609) and minor staurolite characterizes the Lake Chad region. Sample 5607 from Nigeria displays a sharp Ediacaran peak (44% of zircon grains).

In the ergs of central Niger, dune sand is pure quartzose with dominant durable minerals, locally associated with minor garnet or pyroxene (sample 3235). Closer to the eastern side of the Aïr Mountains, some grains of K-feldspar or plagioclase occur and tHM suites locally include common amphibole, epidote, and staurolite. Orosirian zircon ages are slightly more common in this region and Cambrian ages are also observed (3232) as well as one grain as young as 6 Ma (3233). On the western side of the Aïr Mountains, sand is feldspatho-quartzose with significant polycrystalline quartz, orthoclase, microcline*, and sericitized plagioclase (Fig. 4H). The tHM suite is dominated by amphibole (mostly blue-green hornblende) associated with zircon and epidote. The zircon-age spectrum is also distinct, characterized by a sharp Ediacaran peak (47% of total ages), by secondary Orosirian (24%) and Silurian-Mississippian clusters (320-435 Ma; 19%), and by lack of ages older than the Orosirian.

Pure quartzose sand contains different amounts of ZTR minerals in Burkina Faso south of the Niger River (common epidote), Mali, and Mauritania (locally common epidote or pyroxene with minor garnet, staurolite, and amphibole) (Fig. 4D,G). Amphibole increases close to the Atlantic coast. Sand collected in Burkina Faso yielded a minor cluster of Early-Middle Jurassic detrital-zircon ages (4% of total grains). Zircon grains in Mali and Mauritania yielded a significant number of Orosirian (7-13% of total grains), Rhyacian (7-12%) and Archean ages (3-10%), and only minor Tonian (2-5%) and Stenian ages (≤ 4%).

*5.3. The northern Sahara*

In the northern Sahara, sand composition is more varied. Sand collected along the southern and eastern front of the Anti-Atlas Mountains in Morocco ranges from pure quartzose to litho-quartzose with granitoid, mafic volcanic, sedimentary, or very-low-rank to medium-rank metasedimentary rock fragments (Fig. 4A). The tHM suite includes clinopyroxene associated with epidote, pumpellyite, prehnite, amphibole, and durable ZTR minerals. The obtained zircon ages are mostly Neoproterozoic and Orosirian, with one grain as young as 5 Ma (sample 3269).

Dune sand in the Grand Erg Occidental in Algeria is pure quartzose with dominant durable minerals, whereas dune sand of the Grand Erg Oriental in Algeria and Tunisia is quartzose (Fig. 4E), with K-feldspar including microcline* predominating over plagioclase, and locally dominant garnet (5616) or common amphibole and epidote (Table 1). Zircon grains yielded more Ediacaran ages in the Grand Erg Occidental and more Stenian ages in the Gran Erg Oriental.

In the Ubari Erg of Libya, dune sand is pure quartzose with dominant durable minerals associated with mainly actinolitic amphibole and epidote in the east. Dune sand collected in the Murzuq Erg near the Haruj al Aswad volcanic field (5584), instead, is litho-quartzose carbonaticlastic with a moderately poor tHM suite dominated by clinopyroxene and olivine (Fig. 4C). Orosirian ages of detrital zircon decrease, and Archean ages increase, from west to east across the Libyan desert.

In pure quartzose sand of the Western Desert in Egypt, durable minerals are associated with epidote, garnet, and minor hornblende, staurolite and clinopyroxene. The zircon-age spectrum of sample 5601 in the northwest is similar to those of Libyan sands.

Detrital modes are varied in dune sand collected along the western side of the Nile Valley. In the Aswan area, litho-quartzose carbonaticlastic to quartzose sand contains a moderately poor tHM suite with epidote, amphibole, and clinopyroxene. Dune sand to the north ranges from quartz-rich feldspatho-quartzose, with K-feldspar including microcline* predominating over plagioclase, to litho-quartzose sedimentaclastic, quartzose, and pure quartzose. The very poor to moderately poor tHM suites include durable ZTR minerals associated with epidote, staurolite, hornblende, garnet, locally clinopyroxene, and minor kyanite (Table 1).

## 6. Data analysis

All compositional datasets (petrography, heavy minerals, detrital-zircon geochronology) are remarkably homogeneous, indicating that most Sahara dune sands are either derived from similar sources or have been homogenized through multiple sedimentary cycles. Notable differences in compositional signals do occur, but only related to the local addition of volcanic, orogenic, or different sedimentary detritus (Fig. 4). Otherwise, identifying specific provenances, tracing sediment dispersal, and linking transport pathways with prevailing patterns of atmospheric circulation and wind regimes represents an arduous task. After this visual inspection of the data, we now turn to the multivariate ordination techniques to further investigate our results, in the anticipation that these tools may be able to detect hidden patterns and trends that the naked eye might have missed (Fig. 8).

### *6.1. Petrographic dataset*

Correspondence Analysis of petrographic data (Fig. 8A) highlights the very limited variability of quartz content, with dominance of pure quartzose sand across the Sahara (Table 1). A significant variability is observed for K-feldspar and plagioclase, which show a correlated behaviour. Quartz-rich feldspatho-quartzose samples from the western Aïr mountains, Grand Erg Oriental, and Nile Valley have low P/F ratio (24-29%) and low tHMC index, suggesting recycling of locally exposed sandstones ultimately derived from basement rocks rather than first-cycle supply from crystalline basement. Siltstone and metamorphic lithic grains are more common along the front of the Anti-Atlas in Morocco, reflecting orogenic contributions. Nile Valley and Murzuq Basin sands are enriched in carbonate grains derived from Cenozoic cover strata of the Sahara Metacraton.

### *6.2. Heavy-mineral dataset*

Correspondence Analysis of heavy-mineral data (Fig. 8B) highlights the anti-correlation between durable ZTR minerals and epidote + garnet + amphibole, the triad forming the mineralogical suite typical of metamorphic basements (Garzanti and Andò, 2007). The variability of the ZTR index matches that of quartz, indicating a concordant behaviour of all durable minerals typical of extensively recycled sediments. Epidote, amphibole and garnet are correlated (Fig. 6) and relatively common both west and east of the Aïr Mountains, in the Western Desert of Egypt and along the Nile

Valley, with maxima reached in coastal Mauritania and in the Grand Erg Oriental in Algeria. Sample 5616 is the only garnet-dominated sand. Clinopyroxene content varies widely, being most abundant in the NE Murzuq sample 5584, where it is associated with olivine (Fig. 4C), and in all three Moroccan samples also containing prehnite and pumpellyite (Table 1).

*6.3. Detrital-zircon age dataset*

Besides KDE plots — which basically highlight the ubiquitous Pan-African peak with lesser “Grenvillian” (~1 Ga) and “Eburnean” (~2 Ga) clusters (Fig. 7) thus underscoring the homogeneity of geochronological signatures across the Sahara —, the MDS map allows us to extract additional information from zircon-age distributions (Fig. 8C). Geographically closer samples tend to plot closer to each other, as in Chad  and Mauritania. Hierarchical clustering analysis (Fig. C3 in Appendix C) points to a systematic difference between southeastern Sahara samples, characterized by a more prominent ~1.0 Ga peak, and northwestern Sahara samples, yielding fewer Stenian zircons and characterized by a larger Paleoproterozoic peak and some Paleozoic and Mesozoic ages. Sample 5610 from west of the Aïr Mountains is singled out by the presence of a Paleozoic peak and the virtual lack of ~1.0 Ga grains.

*6.4. Inferences based on combined datasets*

Statistical analysis of single datasets meets only limited success in the attempt to highlight significant regional differences among the remarkably homogeneous provenance signatures of Sahara Desert sand. Within each dataset, dissimilarities are mostly small only excepting the few samples documenting additional sediment contribution from local sources. In such a case of homogeneous data, statistical analysis may easily emphasize minor local anomalies and overstress their significance. Combining framework-petrography, heavy-mineral, and geochronological datasets with multivariate analysis produces visual plots (Fig. 8D, 8F) that help us not only to increase discrimination power but also to verify the consistency of potential artefacts, thus leading to more robust results.

The INDSCAL plot (Fig. 8D) shows that three quarters of our samples have the same petrographic and heavy-mineral fingerprint, preventing any provenance discrimination among them. These samples are widely distributed from Chad to Tunisia and from the Western Desert of Egypt to Mauritania, thus failing to display a definite geographical distribution across the Sahara. Some significant differences are however confirmed, concerning samples collected along the Nile Valley in Egypt and the Anti-Atlas front in Morocco, or in the NE Murzuq Erg (5584) and the Aïr Mountains in western Niger (5610). Sample 5616 from Algeria is singled out by its garnet-dominated tHM suite. In the GPA plot (Fig. 8F), clusters were based on the hierarchical clustering dendrogram (Fig. 8E), but addition of detrital-zircon ages does not change the overall picture substantially, maintaining the difference between NW Sahara and SE Sahara samples documented by MDS analysis of the zircon-age dataset. The distinctive local provenance of samples collected along the Anti-Atlas front in Morocco (3269), in the Grand Erg Oriental (5616), in the NE Murzuq Erg (5584), and west of the Aïr Mountains (5610) is confirmed. Other samples from Tunisia (5611), Mauritania (5600), and Chad (5602) have no peculiar petrographic or heavy-mineral fingerprint and they are singled out mainly by subtle differences in their zircon-age spectra (further statistical analysis is presented in Appendix C). This is thus considered either of local significance or as one case of artefact produced by the statistical algorithm (i.e., a false positive) which, in the search of a signal, ends up emphasizing noise.

Even a thorough analysis conducted with sophisticated statistical techniques including Multidimensional scaling (MDS), Correspondence analysis (CA), Individual Difference Scaling (INDSCAL), and General Procrustes Analysis (GPA), therefore, could not break the compositional homogeneity of Sahara dune sands. Rather, the power of these techniques to reveal even the most subtle trend in a large dataset carries the risk of producing spurious results caused by local factors such as wind sorting or bias in sampling or analytical procedures.

*6.5. Local sediment sources*

Petrographic, heavy-mineral, and geochronological signatures and their remarkable homogeneity indicate that Saharan sands have an overwhelmingly multicyclic origin, as discussed in detail in section 7 below. Among the few differences highlighted by statistical analysis (Fig. 8), the two samples consistently displaying a distinct compositional fingerprint are those from the northeastern Murzuq basin (5584) and western Niger (5610).

The NE Murzuq sample is the richest in limestone grains, transparent heavy minerals, clinopyroxene, and olivine of our entire sample set. The contrasting information provided by petrographic and heavy-mineral analyses represents an apparently paradoxical case, which is produced whenever recycled detritus generated by a heavy-mineral poor sedimentary source mixes with minor quantities of first-cycle detritus supplied by a heavy-mineral rich source (figure 1 in Garzanti and Andò, 2019). In this case, local sedimentary sources as young as Quaternary (Geyh and Thiedig, 2008) also supply limestone grains, whereas the Plio-Quaternary Haruj al Aswad basaltic field (Al-Hafdh and Elshaafi, 2015) contributes clinopyroxene and olivine but very few basaltic grains.

The sample collected west of the Aïr mountains (5610) is most distinct in all respects. It is the richest in feldspars and amphibole and yielded only two zircon grains in the entire 654-1569 Ma age range. Rather than additional first-cycle contribution from basement rocks such as the Assodé-Issalane amphibolite-facies metamorphic rocks or Renatt granite, the low P/F ratio and very low heavy-mineral concentration point at recycling of (i.e., derivation from) Paleozoic to Mesozoic sandstones exposed nearby (e.g., Salze et al., 2018).

Moroccan samples document additional contribution from local orogenic sources represented by the High Atlas and adjacent Anti-Atlas Mountains, including clinopyroxene from volcanic rocks and epidote, prehnite, and pumpellyite from very-low to low-grade metavolcanic rocks. Prehnite and pumpellyite are peculiar of this region, and do not occur in the similar tHM suite characterizing the northwestern El Djouf Erg of central Mauritania, which includes more ZTR minerals and less clinopyroxene.

The enrichment in garnet in dune sample 5616 collected in the middle of the Grand Erg Oriental is puzzling (Table 1). This anomaly might be ascribed to local concentration of garnet by selective removal of lower-density minerals, a process that may occur in this dune field characterized by turbulent wind circulation. The widespread presence of star dunes in the erg (Telbisz and Keszler, 2018) lends support to this hypothesis.

Distinct composition also characterizes dunes along the Nile Valley, which include a few feldspars, carbonate rock fragments and a few other sedimentary, metasedimentary and volcanic lithics, together with a tHM suite ranging up to moderately poor and including epidote, amphibole, clinopyroxene, staurolite, and minor garnet and kyanite. This indicates sediment mixing from various sources, including the Saharan Metacraton, its Mesozoic to Cenozoic cover strata, and the Nile (Garzanti et al., 2015a).

### *6.6. Local sediment reworking*

The considerations made above concern only sand derived from lithified source rocks. In desert environments, however, the incessant wind action causes repeated and extensive reworking of unconsolidated sediment, not only from the stoss side to the lee side of active dunes or from one active dune to the next, but also from locally exhumed fossil dune fields. Major sources of wind-reworked sediment are dry lake beds, found in diverse areas both within and at the periphery of the desert and representing the record of a recent wetter past (Drake et al., 2011). Examples include the active dunes dominated by gypsum grains found around Chott el Jerid at the northern edge of the Sahara in Tunisia (Fig. 4B) and the abundant rounded mudclasts mixed with monocrystalline quartz in dunes surrounding the Bodélé Depression in Chad (Fig.4F). Sediment deflated from lake beds, however, dominantly consists of fine silt carried thousands of kilometers away as far as South America and the Caribbean (Swap et al., 1992; Prospero, 1996).

## 7. Polycyclic nature of Saharan sands

### 7.1. Sand derived from sandstone

Saharan dune sand is almost invariably pure quartzose with very poor tHM suites dominated by zircon, tourmaline, and rutile (Fig. 4, 5). Because these are the most mechanically and chemically durable common minerals, and hence those most likely to survive more than a single sedimentary cycle, quartz abundance and depleted tHM suites have long been used as indicators of the extent of recycling (e.g., Hubert, 1962; Blatt, 1967). The monotonous mineralogical signature of dune sand all across the Sahara thus points at provenance dominantly from siliciclastic rocks widely exposed throughout the region and ranging in age from Paleozoic (Avigad et al., 2005; Meinhold et al., 2011; Morton et al., 2011) to Mesozoic (e.g., "Nubian sandstone"; Selley, 1997; Carr, 2003), and Cenozoic (Swezey, 2009).

Detrital-zircon geochronology studies of these sandstones (Table 2) documented the widespread abundance of Neoproterozoic-aged zircon grains, indicating ultimate supply from the Pan-African orogen including the Trans-Sahara belt. A subordinate Paleoproterozoic cluster was inferred to indicate provenance from the West African Craton or perhaps Amazonia (Linnemann et al., 2011). A Tonian age cluster characterizes feldspar-bearing Cambrian sandstones in Morocco (Avigad et al., 2012). The common occurrence of ~1 Ga ("Grenvillian") zircons in Paleozoic to Mesozoic sandstones of southern Libya, lacking equivalents in igneous basements of northern Africa, has been emphasized (Meinhold et al., 2011).

### 7.2. Comparing compiled datasets

Statistical tools are here applied to compare zircon-age data obtained on modern sands (Fig. 9) with compiled age spectra from potential Paleozoic to Mesozoic parent sandstones exposed in northern Africa (Fig. 10). The stack of KDE plots highlights the recurrence of the most prominent Ediacaran (~0.6 Ga) peak in all compiled datasets (Fig. 10B). Among potential source rocks, most distinct is the spectrum from Paleozoic-Mesozoic sandstones of southern Libya (Meinhold et al., 2011), which display more prominent "Grenvillian" (~1 Ga), "Eburnean" (~2 Ga) and "Liberian" (Neoarchean) peaks. More and slightly older Eburnean-aged zircons characterize Cambrian sandstones from western Algeria (Wang et al., 2020). Most striking is the similarity of zircon-age spectra between modern Saharan and Arabian dune sands. Besides the not many Mesozoic and Cenozoic zircons occurring in dune fields close to Arabian Gulf shores and derived from the Anatolia Plateau and the Zagros Mountains *via* the Euphrates-Tigris-Karun river system (Garzanti et al., 2016), differences are limited to a few more ages around 0.8 Ga (a feature common to Nile sand; Fig. 9) and a few more Neoarchean ages in Arabia.

The remarkable homogeneity of detrital-zircon age spectra all across Arabia and northern Africa is confirmed by Multidimensional Scaling analysis. The central position of Saharan sands in MDS maps (Fig. 10C,D) confirm that, as Arabian desert sands, they largely resulted from the homogenization of detritus recycled from Paleozoic to Mesozoic parent sandstones. The MDS maps highlight that this averaged zircon-age signal also characterizes Cambrian sandstones of southeastern Algeria, Morocco, and central-western Libya (Linnemann et al., 2011; Avigad et al., 2012; Altumi et al., 2013), whereas Paleozoic-Mesozoic sandstones of southern Libya (Meinhold et al., 2011) and Cambrian sandstones from western Algeria (Wang et al., 2020) are distinct.

*7.3. Paleozoic sandstones as a major sand supplier for modern dunes*

Cambro-Ordovician and younger sandstones widely exposed across the Sahara represent a huge reservoir of quartz grains to be recycled through time, finally ending up in modern dune fields. In Saharan dune sand, zircon grains yielded mostly (77%) Neoproterozoic ages, consistently with ultimate origin from the Pan-African orogen and the Trans-Sahara belt. Virtually the same zircon-age spectra characterize dune sand across the Sahara, Nile River sand from Ethiopia and Sudan to Egypt, and Arabian sand seas from the Great Nafud in the north to the giant Rub' al Khali in the south (Fig. 9).

Such a vast areal distribution of parent sandstones and daughter sands with similar mineralogical and geochronological fingerprints reflects multiple recycling and homogenization at the wide spatial scale of the whole northern Africa and Middle East throughout the Phanerozoic. After the major Pan-African mountain-building event and the tectonic activity that followed (e.g., Stern, 1985), the large volume of newly produced crustal material was extensively eroded and repeatedly recycled until the present day.

Besides the dominant Neoproterozoic double peak, Meinhold et al. (2013) noted that Grenvillian-aged zircons become more common from Morocco and Algeria to Libya, and from Cambrian to Middle Ordovician strata in Libya. Such an eastward trend is reflected in zircon-age spectra of dune sand, showing a southeastward increase in the relative abundance of Stenian-age zircons from Mali, Mauritania, western Niger and Morocco (≤5% of total ages) to central-eastern Niger, Chad, Libya, and Egypt (3-16% of total ages; Fig. 7).

## 8. Relationships between sand mineralogy and sedimentary processes in desert environments

The origin of sand in large dune fields represents a still poorly understood controversial issue. In many Earth's deserts, aeolian sand is enriched in most durable quartz and ZTR minerals (Muhs, 2004), but such a simple monotonous compositional signature hardly facilitates interpretation, because it is the resultant of the combined effects of diverse processes accumulated through geological time (Dott, 2003). Prominence of physical factors or of chemical processes? Selective break-down of less durable grains by mechanical abrasion, pre-depositional weathering, or intrastratal dissolution? This is the crux of the "quartzarenite problem" (Basu, 2020).

In this section, we review the relationships between sand mineralogy and sedimentary processes in desert environments, placing emphasis on *in situ* sand generation by wind erosion *versus* external fluvial supply. In the former case, most sand results from disaggregation of rocks with high sand-generation potential, such as sandstones or locally granites, and will thus be primarily composed of quartz and locally feldspars with generally very poor heavy-mineral suites largely consisting of ZTR minerals. In the latter case, mineralogy is variable, with larger percentages of first-cycle detritus derived from a wide range of source rocks, including lithic fragments as well as amphibole, epidote, garnet, or pyroxene.

### *8.1. Wind-fed quartz-rich sand seas*

Sand seas consisting of pure quartzose sand are well documented in the Paleozoic (e.g., Dott et al., 1986), Mesozoic (e.g., Bertolini et al., 2020), and Cenozoic (e.g., Vainer et al., 2018). Although the Sahara has several predecessors in geological history, characterized by the same monotonous compositional signature dominated by the most durable minerals, the Sahara cannot be considered the rule in this respect, but rather an end-member case.

The debate on the existence of first-cycle quartzarenites went on for long (Krynine, 1941; Suttner et al., 1981; Johnsson, 1993), until the modern-sand lesson indicated unambiguously that sand consisting virtually entirely of quartz and ZTR minerals cannot be the result of mechanical or weathering processes even in the most aggressive climatic conditions met in modern Earth, but that the final cleansing of less stable minerals requires extensive intrastratal dissolution, i.e., inheritance from previous sedimentary cycles of weathering and diagenesis (Garzanti et al., 2019a). Pure quartzose composition thus implies that sand originated from homogenization of detritus chiefly produced by physical disaggregation of quartz-rich parent sandstones, possibly derived in turn from older granparent sandstones, along a line of ancestry rooted in the deep past.

The Sahara is an example of a vast desert hosting sand purified during multiple steps through Phanerozoic time. No clear trace is left of sediment supplied by rivers draining towards the desert, with the exception of Moroccan dunes at the foot of the Anti-Atlas Mountains and of pyroxene-enriched Egyptian dunes near Aswan and east of the Nile (Garzanti et al., 2015a p.45). Conversely, aeolian sand is overwhelming. Rather than the river supplying sand to the desert, it is the dune field that commonly invades and chokes the dry river valley, as seen in northeastern Egypt and Sinai (Garzanti et al., 2015a p.46). In hyperarid climate, river action may be weakened to the point that fluvial contribution to the dune field becomes insignificant, as documented in northern Arabia, where sand is dominantly supplied by disaggregation of Cambro-Ordovician quartzarenites and no river influences the mineralogy of dune sand if not minimally (< 5%) and near the site where it empties into the desert (Garzanti et al., 2013 p.13).

### *8.2. River-fed lithic-bearing sand seas*

The opposite end-member is represented by sand seas supplied by a major river, as indicated by sand mineralogy maintaining the same characteristic fingerprints of the fluvial feeding system through distances up to a thousand of kilometers. These deserts can be considered as wind-reworked inland or coastal deltas. An emblematic case is represented by the coastal ergs of southwestern Africa, which are mostly fed *via* northward littoral drift from the Orange River mouth. Dune sand of the coastal Namib Erg (southern Nambia) is estimated to be 99% derived from the Orange River even at its farthest northern edge, the main mineralogical and textural differences being a slightly enrichment in quartz at the expense of most easily destroyed sedimentary and metasedimentary lithics, a dearth of mica, and a markedly higher degree of grain roundness (Garzanti et al., 2012, 2015b). Because of hyperarid climate, additional fluvial supply is limited along the coast. Consequently, coastal ergs in northern Nambia to southern Angola are still dominantly derived (~80% and ~60%, respectively) from the Orange River mouth after a mutistep longshore transport up to 1800 km (Garzanti et al., 2014a, 2018c). All along, composition of dune sand remains constantly feldspatho-quartzose with common basaltic rock fragments and rich tHM suites containing high, although progressively diluted, percentages of clinopyroxene.

Fluvial-dominated dune fields tend to be the rule in orogenic settings. Several examples are documented in arid inland areas across Asia, where river sediments are trapped in subsiding troughs adjacent to the front of active orogens such as the Kopeh-Dagh, Kun Lun, Altyn Tagh, Tian Shan, or the western Himalaya. The Karakum Desert in Turkmenistan contains feldspatho-litho-quartzose dune sand with varied lithic population and moderately rich epidote-amphibole-garnet tHM suite, which closely matches sand of the Amu Darja River draining the western Pamir mountains of Tajikistan (Garzanti et al., 2019b).

Dune sand of the Thal Desert in central Pakistan contains subequal amounts of quartz, feldspars, and mostly metamorphic and sedimentary lithic fragments, as well as a very rich amphibole-epidote-garnet-pyroxene tHM suite (Liang et al., 2019). This low-quartz signature indicates supply from the upper Indus River at latest Pleistocene/ealy Holocene times, when erosion was focused on the high mountains of northern Pakistan (Garzanti et al., 2020).

The large Taklamakan Desert of northwestern China contains feldspatho-litho-quartzose sand with mainly sedimentary and metamorphic lithics and moderately rich amphibole-epidote-pyroxene tHM suite, a composition virtually indistinguishable from sand of the Yarkhand River draining the northern Karakorum and Kun Lun Mountains (Rittner et al., 2016).

### *8.3. Fluvial/aeolian connectivity in arid environments*

The interaction between fluvial supply and wind reworking is documented at the periphery of all sand seas. Excellent examples are represented by the eastward landward side of Namibian deserts, where the confict between persistent wind action and episodic river floods produces spectacular sedimentary features (Stanistreet and Stollhofen, 2002; Svendsen et al., 2003; Feder et al., 2018). In the Kalahari Desert, Sahara's brother in southern hemisphere Africa, dune sand is also largely pure quartzose but composition is not equally homogeneous, and distinct mineralogy in different areas reflects a greater role of fluvial supply (Garzanti et al., 2014b). Kalahari dune fields are best developed west of river channels, suggesting deflation of fluvial sediments by easterly winds during drier periods (Shaw and Goudie 2002). Conversely, rivers have inundated interdune areas and incised their course across dune ridges during wetter periods (Thomas et al. 2000). Quartz grains are commonly well rounded in both dune and river sands, documenting aeolian abrasion at one or more stages of their multistep transport history. Climate-controlled cycling of quartzose sand from the fluvial to the aeolian environment and back has taken place repeatedly in the Kalahari (Thomas and Shaw 2002).

In Saudi Arabia, dune sand remains homogeneously quartz-rich feldspatho-quartzose to quartzose across the Rub'Al Khali, the largest continuous sand sea on Earth, but compositional variations are observed along the desert's rims. Dune sand becomes lithic carbonaticlastic close to the Hadhramaut carbonate tableland in Yemen to the south and quartzo-lithic carbonaticlastic along the Gulf shores of the Emirate of Abu Dhabi to the northeast (Garzanti et al., 2001, 2003). Fluvial interactions are documented at the southwestern edge of the sand sea, where dune sand is less quartz-rich than in Cambro-Ordovician parent sandstones, has distinctly higher heavy-mineral concentration, higher amphibole, and lower ZTR indices, indicating that *wadi*-derived first-cycle detritus from the crystalline basement accounts for ~20% of aeolian sand (Garzanti et al., 2017).

Fluvial-aeolian connectivity is well documented in the Thar Desert of southern Pakistan, where sand was exchanged over spatial scales of hundreds of kilometers between the Indus River and the desert. Summer monsoon winds recycle sediment from the lower Indus River and delta downwind and upstream. Large volumes of sediment were thus stored inland since the mid-Holocene, when the desert expanded as the summer monsoon rainfall decreased, buffering the sediment flux to the ocean (East et al., 2015).

Another renowned example of fluvial-aeolian interaction is provided by the sand seas and loess plateau of northern China, where the accumulated sand and dust have been largely transported originally by the Yellow River from the northern Tibetan Plateau (Stevens et al., 2013; Nie et al., 2015). Contrariwise, aeolian sediment is widely supplied to the Yellow River in Inner Mongolia, where the river course is largely incised within loess deposits and flanked by a wide desert area from where aeolian sand is blown periodically toward the fluvial channel by the winter monsoon (Pang et al., 2018). Such a multistep, back-and-forth sediment mixing contributes to extensive homogenization of compositional fingerprints of fluvial sand, dune sand, and loess deposits.

### *8.4. Aeolian processes able to modify sand mineralogy and texture*

Distinguishing end-member types of deserts may appear as a largely conceptual exercise, because landscapes evolve through time under the complex effects of climate change, which controls wind strength, fluvial runoff, water-table level, and vegetation cover. Despite Nature's complexities, however, a basic distinction holds between river-fed sand seas with varied mineralogy including first-cycle detritus (most typical of orogenic settings) *versus* sand seas fed in *situ* by recycling of older sandstones and characterized by distilled composition dominated by quartz and ZTR minerals (most typical of anorogenic settings).

Because arid climate hampers the effectiveness of chemical reactions, processes that can alter sediment composition within a desert are essentially physical, including abrasion and wind sorting. Recycling *per se* can only replicate the mineralogy of parent clastic units in the daughter sand, but by this fundamentally physical mechanism the effects of selective chemical and mechanical breakdown of labile grains can be accumulated through multiple sedimentary cycles, and inherited in the next (Garzanti, 2017).

As a most evident effect of mechanical abrasion and comminution, softer detrital grains effectively increase their roundness in aeolian dunes as a consequence of repeated impacts with harder grains in air (Resentini et al., 2018). Clear examples are seen in the Rub'al Khali, where carbonate grains are most readily rounded with transport distance, progressively reduced in size, and finally removed. Other minerals, cleaved or softer than quartz or garnet like feldspars, rock fragments or ferromagnesian silicates, may also be selectively comminuted and concentrated in finer size fractions (Garzanti et al., 2017).

Selective entrainment and winnowing are other physical processes that can markedly affect sand mineralogy. Deflation by strong winds selectively removes slow-settling detrital components, leaving behind coarser layers (e.g., granule ripples) or laminae enriched in ultradense minerals such as garnet and magnetite. Contrary to mechanical abrasion and comminution, these modifications are largely temporary and reversible.

## 9. Conclusions

The Sahara is a vast desert. Its composite structure includes large dune fields hosted in sedimentary basins separated by elevated areas exposing the roots of Precambrian orogens or created by recent intraplate volcanism. Such an heterogeneity of landscapes and geological formations is contrasted by a remarkably homogeneous composition of dune sand, consisting almost everywhere of > 95% quartz and durable minerals such as zircon, tourmaline, and rutile. Exceptions are recorded only locally in the vicinity of volcanic fields (e.g., Haruj al Aswad in Libya), basement highs (e.g., Aïr Mountains in Niger), fold belts (Anti-Atlas in Morocco), or along the Nile Valley. Everywhere else, from Lake Chad and the Bodélé Depression to the great ergs of Algeria, and from the Western Desert of Egypt to the Atlantic coast of Mauritania, dune sand has almost the same, monotonous, pure quartzose composition. Besides U-Pb age spectra of detrital zircons, which reveal a significant difference between the southeastern part of the desert characterized by a more pronounced ~1 Ga peak *versus* the northwestern part where Paleoproterozoic ages are more common and some Paleozoic and Mesozoic ages occur, our data do not show any compositional trend that could be compared with the main directions of present or past atmospheric circulation and wind transport.

The composition and homogeneity of Saharan dune sand reflect similar generative processes and source rocks, and extensive recycling repeated through geological time after the end of the Neoproterozoic, which zircon-age spectra indicate as the last major event of crustal growth in the region. Subsequently, the newly formed Arabian-Nubian Shield was covered by quartz-rich siliciclastic sediments extending all across the area from Oman to Mauritania and beyond. It is from this thick blanket of sandstone that large volumes of quartzose sand were generated, and enriched progressively in durable minerals during the multiple cycles of erosion, sedimentation and diagenesis that took place in the long period of relative tectonic quiescence that characterized the entire Phanerozoic in this region. The geographic zircon-age distribution in daughter sands thus chiefly reflects the zircon-age distribution in parent sandstones (i.e., different patterns between southeast and northwest), and hence sediment dispersal systems existing at those times rather than present wind patterns (i.e., separation of sand flow between north and south).

Because zircon is durable, the larger part of zircon grains contained in most sediment samples is likely to be recycled from sedimentary covers rather than derived first-cycle from basement rocks. In provenance studies based on detrital-zircon ages, the assumption that observed age patterns reflect transport pathways existing at the time of deposition rather than inheritance from even multiple and remote landscapes of the past thus needs to be carefully investigated and convincingly demonstrated rather than implicitly assumed.

## ACKNOWLEDGMENTS

We warmly thank Charlie Bristow, Luca Baglioni, Raffaele Bitonte, Stefano Del Fraro, Riccardo Graziadei, Laura Fielding, Yani Najman, Ada Ali Abdel Megid, and Diego Roncoroni for providing samples from various Saharan dune fields. Editor Chris Fielding and reviewers Abhijit Basu, Tim Lawton, Luca Caracciolo, and Anonymous#4 provided very careful constructive critical advice. This study was supported by MIUR – Dipartimenti di Eccellenza 2018–2022, Department of Earth and Environmental Sciences, University of Milano-Bicocca. TB is supported by the Natural Environment Research Council through grant NE\L002485\1.

## SUPPLEMENTARY MATERIALS

Supplementary data associated with this article, to be found in the online version at http://dx.doi.____________, include information on sampling sites (Table A1) together with sand-petrography (Table A2) and heavy-mineral data (Table A3). The complete detrital-zircon geochronology dataset is presented in Appendix B. Additional statistical tools are illustrated in Appendix C. The Google-Earth™ map of sampling sites Sahara.kmz is also provided.

## FIGURE AND TABLE CAPTIONS

**Figure 1**. The Sahara Desert in northern Africa. Main dune fields, sedimentary basins, and geological domains are indicated. Sampling sites are shown with circles coloured by region. CeJ = Chott el Jerid (Tunisia); HaA = Haruj al Aswad (Libya).

**Figure 2.** Sand flow patterns obtained by interpolation of metereological and bedform data (grain-size range 50-100 µm; modified after Wilson, 1971). The calculated divide (dashed red line) nearly corresponds to the southern boundary of the subtropical high-pressure zone; peaks P1 (Tademait), P2 (Hoggar), and P3 (Libyan) correspond to high-pressure centres from which sand flow radiates, and saddles S1 (Erg Chech), S2 (Tanezrouf), and S3 (Teneré) correspond to possible sand flow corridors. Mountain areas in brown, with indicated highest elevation for each; sample locations coloured as in Fig. 1.

**Figure 3.** Geology of the Sahara (modified after CGMW-BRGM, 2016). Major tectonic domains are separated by dashed lines. Sample locations coloured as in Fig. 1. ANS = Arabian-Nubian Shield.

**Figure 4.** Compositional variability of Saharan dune sand (photos arranged in geographical order from NW to SE). **A**) Common sedimentary/low-rank metasedimentary lithics (*Ls, Lms*) with minor microlitic volcanic rock fragments (*Lv*) and perthitic K-feldspar (*K*) derived from nearby orogenic sources. **B**) Gypsum clasts (*g*) reworked from the adjacent salt lake. **C**) Common limestone grains (*e* = echinoid spine) with clinopyroxene (*p*) and olivine (*o*) derived from the Haruj al Aswad basaltic field. **D**) Common polycrystalline quartz (*Qp*) associated with up to well-rounded or etched monocrystalline quartz. **E**) Up to well-rounded or etched quartz associated with plagioclase (*P*) and K-feldspar (*K*). **F**) Up to well-rounded quartz with abundant mudclasts (*m*) reworked from the dry bed of once Mega-Lake Chad. **G**) Dominant, up to well-rounded monocrystalline quartz. **H**). Common K-feldspar (*M* = cross-hatched microcline) and plagioclase (*P*); quartz with abraded

overgrowths (*arrow*) indicates recycled origin. **I**) Dominant, up to well-rounded monocrystalline quartz. All photos with crossed polars; blue bar for scale = 100 µm.

**Figure 5**. Petrography of Sahara dune sand. Most samples are monotonously pure quartzose (*pQ*; plotting in blue fields of QFL and QPK diagrams), with K-feldspar prevailing over plagioclase and negligible lithics. A few samples are quartzose, (*Q*) quartz-rich feldspatho-quartzose (*qFQ*), or quartz-rich litho-quartzose sedimentaclastic (*qLQ*; W of Nile Valley, S of Anti-Atlas in Morocco, NE Murzuq Erg in Libya). Q = quartz; F = feldspars (P = plagioclase; Or* = untwinned K-feldspar: Mic* = cross-hatched microcline); L = lithic fragments (Lm = metamorphic; Lv = volcanic; Ls = sedimentary).

**Figure 6**. Heavy minerals in Saharan dune sand. The biplot highlights that tHM suites are mixtures of three main mineral groups: 1) largely recyled durable ZTR; 2) the orogenic triad amphibole, epidote and garnet; 3) volcanic-derived clinopyroxene and olivine. ZTR minerals are dominant in the southern Sahara, with amphibole and locally staurolite increasing close to the Aïr Mountains in Niger (5610). In the northern Sahara, clinopyroxene occurs more frequently and a clinopyroxene-olivine suite characterizes dunes near the Haruj al Aswad volcanic field in Libya (NE Murzuq Erg, 5584).

**Figure 7**. U-Pb age spectra of detrital zircons (age *vs*. frequencies plotted as Kernel Density Estimates using the *provenance* package of Vermeesch et al., 2016). All samples display the characteristic Neoproterozoic "double-peak", with minor Paleoproterozoic and Archean ages. Paleozoic and Mesozoic clusters occur west of the Air Mountains and in Burkina Faso, respectively. Cenozoic ages are found in Algeria and Mauritania and are locally as young as 5-6 Ma in Morocco and Niger.

**Figure 8.** Multivariate statistical analysis (detailed explanation in subsection 4.4). **A**) CA for petrographic (PT) dataset. **B**) CA for heavy-mineral (HM) dataset. **C**) MDS for detrital-zircon (DZ) ages. **D**) INDSCAL for combined PT and HM datasets. Group configuration is expressed by perpendicular arrows and depict the direction of variability for each dataset. **E**) Hierarchical

clustering dendrogram (height refers to normalised distance units produced by GPA of PT, HM, and DZ datasets; Garzanti and Vermmesch, 2015). **F**) Generalised Procrustes Analysis (GPA) of PT, HM and DZ datasets (symbol shapes refer to cluster analysis in ***E*** and colours to geographical location). For ***A***, ***B***, and ***C***, sample locations are shown on the sand flow map below; clusters refer to hierarchical clustering (Appendix C); axes units are normalised values based on chi-square distance for ***A*** and ***B***, and on Kolmogorov-Smirnov distance for ***C***.

**Figure 9.** U-Pb zircon-age spectra are not only remarkably monotonous all across the Sahara, but do not differ significantly from either Nile sand in Sudan to Egypt or from Arabian desert sands (data after Garzanti et al., 2013, 2017, 2018b; age *vs*. frequencies plotted as Kernel Density Estimates using the *provenance* package of Vermeesch et al., 2016). Zircon grains are massively recycled from post-Pan-African siliciclastic units all across from the Arabian Gulf to the Atlantic Ocean. AHD = Aswan High Dam, closed in 1964.

**Figure 10.** Statistical analysis based on compiled detrital-zircon ages presented in Table 2. **A)** Sample locations and sand flow map**. B**) Cumulative KDE plot of all concordant ages from this study (neon red) compared with KDE plots of compiled datasets (peak height normalized to maximum peak of each dataset; bandwidth maintained constant for all datasets). **C**, **D)** MDS maps comparing the compiled zircon-age datasets with the cumulative age spectrum from this study (***C***), and with age spectra for each sample group presented in Fig. 7 (***D***). Axes units are normalised values based on Kolmogorov-Smirnov distance, with 90% confidence polygons represented by dashed red lines. Solid and dashed black lines link closest and second-closest neighbours, respectively. Shepard's plot shown in lower left corner.

**Table 1**. Petrography and heavy minerals in Saharan dune sands. Q = quartz; F = feldspars (P = plagioclase); L = lithic grains (Lv = volcanic; Lc = carbonate; Lsm = other sedimentary and metasedimentary). Transparent heavy minerals (tHMC) include: ZTR = zircon + tourmaline + rutile; Ap = apatite; Ttn = titanite; Ep = epidote; P&P = prehnite + pumpellyite; Grt = garnet; St = staurolite;

Ky = kyanite; Amp = amphibole; Px = pyroxene; Ol = olivine; &tHM = others (anatase, sillimanite, andalusite, monazite, topaz, brookite). Full information on counted grains is provided in Appendix Tables A2 and A3.

**Table 2**. Compilation of ages of detrital zircons contained in Phanerozoic sedimentary rocks and modern dunes from northern Africa and Arabia. Age range is in Ga and percentage of grain ages are provided for each cluster.

**REFERENCES**

Abdelhak, M., Ahmed, K., Abdelkader, B., Brahim, Z., Rachid, K., 2014. Algerian Sahara sand dunes characterization. Silicon 6, 149-154.

Abdelkareem, M., El-Baz, F., 2015. Regional view of a trans-African drainage system. Journal of Advanced Research 6, 433-439.

Abdelsalam, M.G., 2018. The Nile's journey through space and time: A geological perspective. Earth-Science Reviews 177, 742-773.

Abdelsalam, M.G., Liégeois, J.P., Stern, R.J., 2002. The Saharan Metacraton. Journal of African Earth Sciences 34, 119-136.

Abouchami, W., Boher, M., Michard, A., Albarede, F., 1990. A major 2.1 Ga event of mafic magmatism in West Africa: an early stage of crustal accretion. Journal of Geophysical Research: Solid Earth 95, 17605-17629.

Al-Gamal, S.A., 2011. An assessment of recharge possibility to North-Western Sahara Aquifer System (NWSAS) using environmental isotopes. Journal of Hydrology, 398, 184-190.

Al-Hafdh, N.M., Elshaafi, A.E.S.S., 2015. Geochemistry and petrology of basic volcanic rocks of Jabal Al Haruj Al-Aswad, Libya. International Journal of Geosciences 6, 109-144.

Altumi, M.M., Elicki, O., Linnemann, U., Hofmann, M., Sagawe, A., Gärtner, A., 2013. U–Pb LA-ICP-MS detrital zircon ages from the Cambrian of Al Qarqaf Arch, central-western Libya: Provenance of the West Gondwanan sand sea at the dawn of the early Palaeozoic. Journal of African Earth Sciences 79, 74-97.

Andò, S., 2020. Gravimetric separation of heavy-minerals in sediments. Minerals 10(3), 273, doi:10.3390/min10030273.

Arbuszewski, J.A., deMenocal, P. B., Cléroux, C., Bradtmiller, L., Mix, A., 2013. Meridional shifts of the Atlantic intertropical convergence zone since the Last Glacial Maximum. Nature Geoscience 6, 959-962.

Avigad, D., Sandler, A., Kolodner, K., Stern, R. J., McWilliams, M., Miller, N., Beyth, M., 2005. Mass-production of Cambro–Ordovician quartz-rich sandstone as a consequence of chemical weathering of Pan-African terranes: environmental implications. Earth and Planetary Science Letters 240, 818-826.

Avigad, D., Gerdes, A., Morag, N., Bechstädt, T., 2012. Coupled U–Pb–Hf of detrital zircons of Cambrian sandstones from Morocco and Sardinia: implications for provenance and Precambrian crustal evolution of North Africa. Gondwana Research 21, 690-703.

Bagnold, R.A., 1942. The physics of blown sand and desert dunes. Methuen & Co., Ltd., London, 265 p.

Baird, T., Bristow, C. S., Vermeesch, P., 2019. Measuring Sand Dune Migration Rates with COSI-Corr and Landsat: Opportunities and Challenges. Remote Sensing 11, 2423.

Bakker, N.L., Drake, N.A., Bristow, C.S., 2019. Evaluating the relative importance of northern African mineral dust sources using remote sensing. Atmospheric Chemistry and Physics 19(16), 10525–10535.

Basu, A., 2020. Chemical weathering, first cycle quartz sand, and its bearing on quartz arenite. Journal Indian Association of Sedimentologists 37(2), 3-14.

Bertolini, G., Marques, J.C., Hartley, A.J., Da- Rosa, A.A., Scherer, C.M., Basei, M.A., Frantz, J.C., 2020, Controls on Early Cretaceous desert sediment provenance in south- west Gondwana, Botucatu Formation (Brazil and Uruguay). Sedimentology 67(5), 2672-2690.

Bertrand, J.M.L., Caby, R., 1978. Geodynamic evolution of the Pan-African orogenic belt: a new interpretation of the Hoggar shield (Algerian Sahara). Geologische Rundschau 67, 357-388.

Bird, P., 1979. Continental delamination and the Colorado Plateau. Journal of Geophysical Research 84, 7561-7571.

Birkett, C. M., 2000. Synergistic remote sensing of Lake Chad: Variability of basin inundation. Remote sensing of Environment 72, 218-236.

Black, R., 1965. Sur la signification pétrogénétique de la découverte d'anorthosites associées aux complexes subvolcaniques du Niger. Comptes rendus de l'Académie des Sciences 260, 5829-5832.

Black, R., Caby, R., Moussine-Pouchkine, A., Bayer, R., Bertrand, J.M., Boullier, A.M., Fabre, J., Lesquer, A., 1979. Evidence for late Precambrian plate tectonics in West Africa. Nature 278, 223-227.

Blatt, H., 1967. Provenance determinations and recycling of sediments. Journal of Sedimentary Petrology 37, 1031-1044.

Boullier, A.M., Rocci, G., Cosso, N.Y., 1991. La chaîne pan-africaine d'Aouzegeur en Aïr (Niger): un trait majeur du bouclier Touareg. Comptes rendus Académie des Sciences de Paris 313, 63-68.

Breed, C.S., Fryberger, S.G., Andrews, S., McCauley, C., Lennartz, F., Gebel, D., Horstman, K., 1979. Regional studies of sand seas using Landsat (ERTS) imagery. A study of global sand seas. US Geological Survey, Professional Paper 1052, 305-397.

Brenchley, P.J., Marshall, J.D., Carden, G.A.F., Robertson, D.B.R., Long, D.G.F., Meidla, T., Hints, L., Anderson, T.F., 1994. Bathymetric and isotopic evidence for a short-lived Late Ordovician glaciation in a greenhouse period. Geology 22, 295-298.

Bristow, C.S., Armitage, S.J., 2016. Dune ages in the sand deserts of the southern Sahara and Sahel. Quaternary International 410, 46-57.

Bristow, C.S., Drake, N., Armitage, S., 2009. Deflation in the dustiest place on Earth: the Bodélé Depression, Chad. Geomorphology 105, 50-58.

Bumby, A.J., Guiraud, R., 2005. The geodynamic setting of the Phanerozoic basins of Africa. Journal of African Earth Sciences 43, 1-12.

Burke, K., 1999. Tectonic significance of the accumulation of the voluminous early Paleozoic reservoir containing quartz-rich sandstones of North Africa and Arabia. Bulletin of the Geological Society Houston, 11-13.

Caby, R., Andreopoulos-Renaud, U., Pin, C., 1989. Late Proterozoic arc–continent and continent–continent collision in the Pan-African Trans-Saharan Belt of Mali. Canadian Journal of Earth Sciences 26, 1136-1146.

Caby, R., Bertrand, J.M.L., Black, R., 1981. Pan-African ocean closure and continental collision in the Hoggar-Iforas segment, central Sahara. Precambrian Plate Tectonics 16, 407-434.

Capot-Rey, R., 1945. Dry and humid morphology in the Western Erg. Geographical Review 35, 391-407.

Carr, I.D., 2003. A sequence stratigraphic synthesis of the North African Mesozoic. Journal of Petroleum Geology 26, 133-152.

Carroll, J.D., Chang, J.J., 1970. Analysis of individual differences in multidimensional scaling via an N-way generalization of Eckart–Young decomposition. Psychometrika 35, 283–319.

CGMW-BRGM, 2016.Geological Map of Africa, 1:10 million scale. Thiéblemont, D. et al. (eds.), www.brgm.fr.

Chikhaoui, M., Dupuy, C., Dostal, J., 1978. Geochemistry of late Proterozoic volcanic rocks from Tassendjanet area (N.W. Hoggar, Algeria). Contributions to Mineralogy and Petrology 66, 157-164.

Coe, M.T., Foley, J.A., 2001. Human and natural impacts on the water resources of the Lake Chad basin. Journal of Geophysical Research: Atmospheres 106, 3349-3356.

Coward, M. P., Ries, A. C., 2003. Tectonic development of North African basins. Geological Society, London, Special Publications 207, 61-83.

Crouvi, O., Schepanski, K., Amit, R., Gillespie, A.R., Enzel, Y., 2012. Multiple dust sources in the Sahara Desert: The importance of sand dunes. Geophysical Research Letters 39, L13401, doi:10.1029/2012GL052145.

Cvetković, V., Toljić, M., Ammar, N.A., Rundić, L., Trish, K. B., 2010. Petrogenesis of the eastern part of the Al Haruj basalts (Libya). Journal of African Earth Sciences 58, 37-50.

deMenocal, P., Ortiz, J., Guilderson, T., Adkins, J., Sarnthein, M., Baker, L., Yarusinsky, M., 2000. Abrupt onset and termination of the African Humid Period: Rapid climate responses to gradual insolation forcing. Quaternary Science Reviews 19, 347-361.

Denkler, T., Franz, G., Schandelmeier, H., 1994. Tectonometamorphic evolution of the Neoproterozoic Delgo suture zone, northern Sudan. Geologische Rundschau 83, 578-590.

Dickinson, W.R., 1985. Interpreting provenance relations from detrital modes of sandstones. In: Zuffa, G.G. (ed.), Provenance of Arenites. Reidel, Dordrecht, NATO ASI Series 148, 333-361.

Dott, R.H., 2003. The importance of eolian abrasion in supermature quartz sandstones and the paradox of weathering on vegetation-free landscapes. The Journal of Geology 111, 387-405.

Dott, R.H., Byers, C.W., Fielder, G.W., Stenzel, S.R., Winfree, K.E., 1986. Aeolian to marine transition in Cambro-Ordovician cratonic sheet sandstones of the northern Mississippi Valley, U.S.A. Sedimentology 33, 345–367.

Drake, N. A., Blench, R. M., Armitage, S. J., Bristow, C. S., White, K. H., 2011. Ancient watercourses and biogeography of the Sahara explain the peopling of the desert. Proceedings of the National Academy of Sciences 108, 458-462.

Dutta, P.K., Zhou, Z., dos Santos, P.R., 1993. A theoretical study of mineralogical maturation of eolian sand. In: Basu, A., Johnsson, M. (eds.), Processes Controlling the Composition of Clastic Sediments. Geological Society of America, Special Paper 284, 203-209.

East, A.E., Clift, P.D., Carter, A., Alizai, A., Van Laningham, S., 2015. Fluvial–eolian interactions in sediment routing and sedimentary signal buffering: an example from the Indus Basin and Thar Desert. Journal of Sedimentary Research 85(6), 715-728.

Echikh, K., 1998. Geology and hydrocarbon occurrences in the Ghadames basin, Algeria, Tunisia, Libya. Geological Society, London, Special Publications 132, 109-129.

El-Baz, F., 1998. Sand accumulation and groundwater in the eastern Sahara. Episodes 21, 147-151.

El-Baz, F., 2000. Satellite observations of the interplay between wind and water processes in the Great Sahara. Photogrammetric Engineering and Remote Sensing 66(6), 777-782.

Elbelrhiti, H., 2012. Initiation and early development of barchan dunes: A case study of the Moroccan Atlantic Sahara Desert. Geomorphology 138, 181-188.

Elshaafi, A., Gudmundsson, A., 2016. Volcano-tectonics of the Al haruj volcanic province, Central Libya. Journal of Volcanology and Geothermal Research 325, 189-202.

Ennih, N. Liégeois, J. P., 2001. The Moroccan Anti-Atlas: the West African craton passive margin with limited Pan-African activity. Implications for the northern limit of the craton. Precambrian Research 112, 291-304.

Ennih, N., Liégeois, J.P., 2008. The boundaries of the West African craton, with special reference to the basement of the Moroccan metacratonic Anti-Atlas belt. Geological Society, London, Special Publications 297, 1-17.

Fabre, J., Ba, H., Black, R., Caby, R., Leblanc, M., Lesquer, A., 1982. La chaîne Pan-Africaine, son avant-pays et la zone de suture au Mali. Carte géologique et gravimétrique de l'Adrar des Iforas au 1/500 000, notice and map. Direction nationale de la Géologie et des Mines, Bamako, 85.

Feder, A., Zimmermann, R., Stollhofen, H., Caracciolo, L., Garzanti, E., Andreani, L., 2018. Fluvial-aeolian sedimentary facies, Sossusvlei, Namib Desert. Journal of Maps 14(2), 630-643.

Fekirine, B., Abdallah, H., 1998. Palaeozoic lithofacies correlatives and sequence stratigraphy of the Saharan Platform, Algeria. Geological Society, London, Special Publications 132, 97-108.

Feller, W., 1948. On the Kolmogorov-Smirnov limit theorems for empirical distributions. Annals of Mathematical Statistics 19, 177-189.

Feybesse, J.L., Milési, J.P., 1994. The Archaean/Proterozoic contact zone in West Africa: A mountain belt of décollement thrusting and folding on a continental margin related to 2.1 Ga convergence of Archaean cratons? Precambrian Research 69, 199-227.

Fezaa, N., Liégeois, J.P., Abdallah, N., Cherfouh, E.H., De Waele, B., Bruguier, O., Ouabadi, A., 2010. Late Ediacaran geological evolution (575–555 Ma) of the Djanet Terrane, Eastern Hoggar, Algeria, evidence for a Murzukian intracontinental episode. Precambrian Research 180, 299-327.

Fezaa, N., Liégeois, J.P., Abdallah, N., Bruguier, O., De Waele, B., Ouabadi, A., 2019. The 600 Ma-old Pan-African magmatism in the In Ouzzal terrane (Tuareg Shield, Algeria): Witness of the metacratonisation of a rigid block. The Geology of the Arab World - An Overview. Springer, Cham., 109-148.

Gabriel, K.R., 1971. The biplot graphic display of matrices with application to principal component analysis. Biometrika 58, 453-467.

Galehouse, J.S., 1971. Point counting. Procedures in sedimentary petrology. Wiley, New York, 385-407.

Gao, H., Bohn, T. J., Podest, E., McDonald, K.C., Lettenmaier, D.P., 2011. On the causes of the shrinking of Lake Chad. Environmental Research Letters 6, 034021.

Garzanti, E., 1991. Non-carbonate intrabasinal grains in arenites: Their recognition, significance and relationship to eustatic cycles and tectonic setting. Journal of Sedimentary Petrology 61, 959-975.

Garzanti, E., 2017. The maturity myth in sedimentology and provenance analysis. Journal of Sedimentary Research 87, 353-365.

Garzanti, E., 2019. Petrographic classification of sand and sandstone. Earth-Science Reviews 192, 545-563.

Garzanti, E., Andò, S., 2007. Plate tectonics and heavy-mineral suites of modern sands. In: Mange, M.A., Wright, D.T. (eds.), Heavy minerals in use. Elsevier, Amstrerdam, Developments in Sedimentology 58, 741-763.

Garzanti, E., Andò, S., 2019. Heavy Minerals for Junior Woodchucks. Minerals 9, 148, doi:10.3390/min9030148.

Garzanti, E., Vezzoli, G., 2003. A classification of metamorphic grains in sands based on their composition and grade. Journal of Sedimentary Research, 73, 830-837.

Garzanti E., Vezzoli G., Andò S., Castiglioni G., 2001. Petrology of rifted-margin sand (Red Sea and Gulf of Aden, Yemen). The Journal of Geology 109, 277-297.

Garzanti, E., Andò, S., Vezzoli, G., Dell'Era, D., 2003. From rifted margins to foreland basins : investigating provenance and sediment dispersal across desert Arabia (Oman, UAE). Journal of Sedimentary Research 73, 572-588.

Garzanti E., Doglioni C., Vezzoli G., Andò S., 2007. Orogenic belts and orogenic sediment provenances. The Journal of Geology 115, 315-334.

Garzanti, E., Andò, S., Vezzoli, G., Lustrino, M., Boni, M., Vermeesch, P., 2012. Petrology of the Namib Sand Sea: Long-distance transport and compositional variability in the wind-displaced Orange Delta. Earth-Science Reviews 112, 173-189.

Garzanti, E., Vermeesch, P., Andò, S., Vezzoli, G., Valagussa, M., Allen, K., Khadi, K.A., Al-Juboury, I.A., 2013. Provenance and recycling of Arabian desert sand. Earth-Science Reviews 120, 1–19.

Garzanti. E., Vermeesch, P., Andò, S., Lustrino, M., Padoan, M., Vezzoli, G., 2014a. Ultra-long distance littoral transport of Orange sand and provenance of the Skeleton Coast Erg (Namibia). Marine Geology 357, 25-36.

Garzanti, E., Vermeesch, P., Padoan, M., Resentini, A., Vezzoli, G., Andò, S., 2014b. Provenance of passive-margin sand (southern Africa). The Journal of Geology 122, 17-42.

Garzanti, E., Andò, S., Padoan, M., Vezzoli, G., El Kammar, A., 2015a. The modern Nile sediment system: Processes and products. Quaternary Science Reviews 130, 9-56.

Garzanti, E., Resentini, A., Andò, S., Vezzoli, G., Vermeesch, P., 2015b. Physical controls on sand composition and relative durability of detrital minerals during long-distance littoral and eolian transport (coastal Namibia). Sedimentology, 62, 971-996, DOI: 10.1111/sed.12169.

Garzanti, E., Al-Juboury, A.I., Zoleikhaei, Y., Vermeesch, P., Jotheri, J., Akkoca, D.B., Allen, M., Andò, S., Limonta, M., Padoan, M., Resentini, A., Rittner, M., Vezzoli, G., 2016. The Euphrates-Tigris-Karun river system: Provenance, recycling and dispersal of quartz-poor foreland-basin sediments in arid climate. Earth-Science Reviews 162, 107-128.

Garzanti E., Vermeesch, P., Al-Ramadan, K.A., Andò, S., Limonta, M., Rittner, M., Vezzoli, G., 2017. Tracing transcontinental sand transport: From Anatolia-Zagros to the Rub' al Khali Sand Sea. Journal of Sedimentary Research 87, 1196-1213.

Garzanti, E., Dinis, P., Vermeesch, P., Andò, S., Hahn, A., Huvi, J., Limonta, M., Padoan, M., Resentini, A., Rittner, M., Vezzoli, G., 2018a. Dynamic uplift, recycling, and climate control on the petrology of passive-margin sand (Angola). Sedimentary Geology 375, 86-104.

Garzanti, E., Vermeesch, P., Rittner, M., Simmons, M., 2018b. The zircon story of the Nile: Time-structure maps of source rocks and discontinuous propagation of detrital signals. Basin Research 30, 1098-1117.

Garzanti, E., Dinis, P., Vermeesch, P., Andò, S., Hahn, A., Huvi, J., Limonta, M., Padoan, M., Resentini, A., Rittner, M., Vezzoli, G., 2018c. Sedimentary processes controlling ultralong cells of littoral transport: Placer formation and termination of the Orange sand highway in southern Angola, Sedimentology 65, 431-460.

Garzanti, E., Vermeesch, P., Vezzoli, G., Andò, S., Botti, E., Limonta, M., Dinis, P., Hahn, A., Baudet, D., De Grave, J., Yaya, N.K., 2019a. Congo River sand and the equatorial quartz factory. Earth-Science Reviews 197, 102918.

Garzanti, E., Ghassemi, M.R., Limonta, M., Resentini, A., 2019b. Provenance of Karakum Desert sand (Turkmenistan): Lithic-rich orogenic signature of central Asian dune fields. Rivista Italiana di Paleontologia e Stratigrafia 125(1), 77-89.

Garzanti, E., Liang, W., Andò, S., Clift, P.D, Resentini, A., Vermeesch, P., Vezzoli, G., 2020. Provenance of Thal Desert sand: Focused erosion in the western Himalayan syntaxis and foreland-basin deposition driven by latest Quaternary climate change. Earth-Science Reviews, 207, 103220.

Gasse, F., 2000. Hydrological changes in the African tropics since the Last Glacial Maximum. Quaternary Science Reviews 19, 189-211.

Geyh, M.A., Thiedig, F., 2008. The Middle Pleistocene Al Mahrúqah Formation in the Murzuq Basin, northern Sahara, Libya: evidence for orbitally-forced humid episodes during the last 500,000 years. Palaeogeography, Palaeoclimatology, Palaeoecology 257, 1-21.

Ghienne, J.F., Desrochers, A., Vandenbroucke, T.R., Achab, A., Asselin, E., Dabard, M.P., Farley, C., Loi, A., Paris, F., Wickson, S., Veizer, J., 2014. A Cenozoic-style scenario for the end-Ordovician glaciation. Nature Communications 5, 1-9.

Ghoneim, E., Robinson, C., El-Baz, F., 2007. Radar topography data reveal drainage relics in the eastern Sahara. International Journal of Remote Sensing 28, 1759-1772.

Ghuma, M.A., Rogers, J.J.W., 1978. Geology, geochemistry, and tectonic setting of the Ben Ghnema batholith, Tebisti Massif, southern Libya. Geological Society America Bulletin 89, 1315–1358.

Gischler, C.E., 1976. Hydrology of the Sahara. Ecological Bulletins, 83-101.

Gossel, W., Ebraheem, A.M., Wycisk, P., 2004. A very large scale GIS-based groundwater flow model for the Nubian sandstone aquifer in Eastern Sahara (Egypt, northern Sudan and eastern Libya). Hydrogeology Journal 12, 698-713.

Goudie, A.S., 2005. The drainage of Africa since the Cretaceous. Geomorphology 67, 437-456.

Gower, J.C., 1975. Generalized procrustes analysis. Psychometrika 40, 33-51.

Greenacre, M., 2017. Correspondence analysis in practice. CRC press, Boca Raton (FL), 327 p.

Griffin, W.L., Powell, W.J., Pearson, N.J., O'Reilly, S.Y., 2008. GLITTER: data reduction software for laser ablation ICP-MS. Laser Ablation-ICP-MS in the earth sciences. Mineralogical association of Canada, short course series 40, 204-207.

Grove, A.T., Warren, A., 1968. Quaternary landforms and climate on the south side of the Sahara. The Geographical Journal 134, 194-208.

Haddoum, H., Guiraud, R., Moussine-Pouchkine, A., 2001. Hercynian compressional deformations of the Ahnet-Mouydir Basin, Algerian Saharan Platform: Far-field stress effects of the Late Paleozoic orogeny. Terra Nova 13, 220-226.

Haug, G.H., Hughen, K.A., Sigman, D.M., Peterson, L.C., Röhl, U., 2001. Southward migration of the intertropical convergence zone through the Holocene. Science 293, 1304-1308.

Hubert, J.F., 1962. A zircon–tourmaline–rutile maturity index and the interdependence of the composition of heavy mineral assemblages with the gross composition and texture of sandstones. Journal of Sedimentary Petrology 32, 440-450.

Ingersoll, R.V., Bullard, T.F., Ford, R.L., Grimm, J.P., Pickle, J.D., Sares, S.W., 1984. The effect of grain size on detrital modes: A test of the Gazzi-Dickinson point-counting method. Journal of Sedimentary Petrology 54, 103-116.

Jackson, S.E., Pearson, N.J., Griffin, W.L., Belousova, E.A., 2004. The application of laser ablation-inductively coupled plasma-mass spectrometry to in situ U–Pb zircon geochronology. Chemical Geology 211, 47-69.

Jewell, A.M., Drake, N., Crocker, A.J., Bakker, N.L., Kunkelova, T., Bristow, C.S., Cooper, M.J., Milton, J.A., Breeze, P.S., Wilson, P.A., 2020. Three North African dust source areas and their geochemical fingerprint. Earth and Planetary Science Letters 554, 116645, doi.org/10.1016/j.epsl.2020.116645.

Johnsson, M.J., 1993. The system controlling the composition of clastic sediments. In: Johnsson, M.J., Basu, A. (eds.), Processes controlling the composition of clastic sediments. Geological Society of America, Special Paper 284, pp. 1–19.

Koren, I., Kaufman, Y.J., Washington, R., Todd, M.C., Rudich, Y., Martins, J.V., Rosenfeld, D., 2006. The Bodélé depression: A single spot in the Sahara that provides most of the mineral dust to the Amazon forest. Environmental Research Letters 1, 01400.

Kruskal, J.B., Wish, M., 1978. Multidimensional scaling. Sage Publications, Newbury Park (CA), Quantitative applications in the social sciences, Sage University Paper Series 07-011, 92 p.

Krynine, P.D., 1941. Paleogeographic and tectonic significance of sedimentary quartzites. Geological Society of America Bulletin 52, 1915–1916.

Kuper, R., Kröpelin, S., 2006. Climate-controlled Holocene occupation in the Sahara: Motor of Africa's evolution. Science 313, 803-807.

Kuster, D., Liégeois, J.-P., 2001. Sr, Nd isotopes and geochemistry of the Bayuda Desert high-grade metamorphic basement (Sudan): An early Pan-African oceanic convergent margin, not the edge of the East Saharan ghost craton. Precambrian Research 109, 1–23.

Lancaster, N., 1995. Geomorphology of desert dunes. Psychology Press.

Lancaster, N., 2020. On the formation of desert loess. Quaternary Research 96, 105-122. 247.

Liang, W., Garzanti, E., Andò, S., Gentile, P., Resentini, A., 2019. Multimineral fingerprinting of Transhimalayan and Himalayan sources to Indus-derived Thal Desert sand (central Pakistan). Minerals, 9, 457; doi:10.3390/min9080457.

Liégeois, J.P., 2019. A new synthetic geological map of the Tuareg Shield: An overview of its global structure and geological evolution. In The Geology of the Arab World - An Overview. Springer, Cham, 83-107.

Liégeois, J.P., Black, R., 1987. Alkaline magmatism subsequent to collision in the Pan-African belt of the Adrar des Iforas (Mali). Alkaline Igneous Rocks 30, 381-401.

Liégeois, J.P., Black, R., Navez, J., Latouche, L., 1994. Early and late Pan-African orogenies in the Aïr assembly of terranes (Tuareg Shield, Niger). Precambrian Research 67, 59-88.

Liégeois, J.P., Latouche, L., Navez, J., Black, R., 2000. Pan-African collision, collapse and escape tectonics in the Tuareg shield: Relations with the East Saharan Ghost craton and the West African craton. Journal of African Earth Sciences 30, 53-53.

Linnemann, U., Ouzegane, K., Drareni, A., Hofmann, M., Becker, S., Gärtner, A., Sagawe, A., 2011. Sands of West Gondwana: An archive of secular magmatism and plate interactions—a case study from the Cambro-Ordovician section of the Tassili Ouan Ahaggar (Algerian Sahara) using U–Pb–LA-ICP-MS detrital zircon ages. Lithos 123, 188-203.

Ludwig, K.R., 1998. On the treatment of concordant uranium-lead ages. Geochimica et Cosmochimica Acta 62, 665-676.

Mainguet, M., 1978. The influence of trade winds, local air-masses and topographic obstacles on the aeolian movement of sand particles and the origin and distribution of dunes and ergs in the Sahara and Australia. Geoforum 9, 17-28.

Mainguet, M., Callot, Y., 1978. L'erg de Fachi-Bilma, Tchad-Niger: contribution à la connaissance de la dynamique des ergs et des dunes des zones arides chaudes. Éditions du Centre national de la recherche scientique.

Mainguet, M., Chemin, M.C., 1983. Sand seas of the Sahara and Sahel: An explanation of their thickness and sand dune type by the sand budget principle. Elsevier, Amsterdam, Developments in sedimentology 38, 353-363.

Mattauer, M., Tapponier, P., Proust, F., 1977. Sur les mécanismes de formation des chaines intracontinentales: L'exemple des chaines atlasiques du Maroc, Bulletin de la Societé Géologique de France 77, 521-526.

Meftah, N., Mahboub, M.S., 2020. Spectroscopic characterizations of sand dunes minerals of El-Oued (Northeast Algerian Sahara) by FTIR, XRF and XRD analyses. Silicon 12, 147-153.

Meinhold, G., Morton, A.C., Fanning, C.M., Frei, D., Howard, J.P., Phillips, R.J., Strogen, D., Whitham, A.G., 2011. Evidence from detrital zircons for recycling of Mesoproterozoic and Neoproterozoic crust recorded in Paleozoic and Mesozoic sandstones of southern Libya. Earth and Planetary Science Letters 312, 164-175.

Meinhold, G., Morton, A.C., Avigad, D., 2013. New insights into peri-Gondwana paleogeography and the Gondwana super-fan system from detrital zircon U–Pb ages. Gondwana Research 23, 661-665.

Middleton, N.J., Goudie, A.S., 2001. Saharan dust storms: nature and consequences. Earth-Science Reviews 56, 179–204.

Moreau, C., Demaiffe, D., Bellion, Y., Boullier, A.M., 1994. A tectonic model for the location of Palaeozoic ring complexes in Air (Niger, West Africa). Tectonophysics 234, 129-146.

Morton, A.C., Meinhold, G., Howard, J.P., Phillips, R.J., Strogen, D., Abutarruma, Y., Elgadry, M., Thusu, B., Whitham, A.G., 2011. A heavy mineral study of sandstones from the eastern Murzuq Basin, Libya: Constraints on provenance and stratigraphic correlation. Journal of African Earth Sciences 61, 308-330.

Muhs, D.R., 2004. Mineralogical maturity in dunefields of North America, Africa and Australia. Geomorphology 59, 247-269.

Muhs, D.R., Bush, C.A., Stewart, K.C., Rowland, T.R., Crittenden, R.C., 1990. Geochemical evidence of Saharan dust parent material for soils developed on Quaternary limestones of Caribbean and western Atlantic islands. Quaternary Research 33, 157-177.

Muhs, D.R., Meco, J., Budahn, J.R., Skipp, G.L., Betancort, J.F., Lomoschitz, A., 2019. The antiquity of the Sahara Desert: New evidence from the mineralogy and geochemistry of Pliocene paleosols on the Canary Islands, Spain. Palaeogeography, Palaeoclimatology, Palaeoecology 533, 109245.

Muhs, D.R., Roskin, J., Tsoar, H., Skipp, G., Budahn, J.R., Sneh, A., Porat, N., Stanley, J.D., Katra, I., Blumberg, D.G., 2013. Origin of the Sinai–Negev erg, Egypt and Israel: Mineralogical and geochemical evidence for the importance of the Nile and sea level history. Quaternary Science Reviews 69, 28-48.

Nance, R.D., Murphy, J.B., Strachan, R.A., Keppie, J.D., Gutiérrez-Alonso, G., Fernández-Suárez, J., Quesada, C., Linnemann, U., D'lemos, R., Pisarevsky, S.A., 2008. Neoproterozoic-early Palaeozoic tectonostratigraphy and palaeogeography of the peri-Gondwanan terranes: Amazonian v. West African connections. Geological Society, London, Special Publications 297, 345-383.

Nicholson, S.E., Flohn, H., 1980. African environmental and climatic changes and the general atmospheric circulation in late Pleistocene and Holocene. Climatic change 2, 313-348.

Nie, J., Stevens, T., Rittner, M., Stockli, D., Garzanti, E., Limonta, M., Bird, A., Andò, S., Vermeesch, P., Saylor, J., Lu, H., Breecker, D., Hu, X., Liu, S., Resentini, A., Vezzoli, G., Peng, W., Carter, A., Ji, S., Pan, B., 2015. Loess Plateau storage of Northeastern Tibetan Plateau-derived Yellow River sediment. Nature Communications, 6, DOI: 10.1038/ncomms9511.

Pachur, H.J., Kröpelin, S., 1987. Wadi Howar: Paleoclimatic evidence from an extinct river system in the southeastern Sahara. Science 237, 298-300.

Pang, H., Pan, B., Garzanti, E., Gao, H., Zhao, X., Chen, D., 2018. Mineralogy and geochemistry of modern Yellow River sediments: Implications for weathering and provenance. Chemical Geology, 488, 76-86.

Pinna, P., Calvez, J.Y., Abessolo, A., Angel, J.M., Mekoulou- Mekoulou, T., Mananga, G., Vernhet, Y., 1994. Neoproterozoic events in Tchollire area: Pan-African crustal growth and geodynamics in central-northern Cameroon (Adamawa and North Provinces). Journal African Earth Sciences 18, 347-353.

Prospero, J.M., 1996. Saharan dust transport over the North Atlantic Ocean and Mediterranean: An overview. In: Guerzoni, S., Chester, R. (eds.), The impact of desert dust across the Mediterranean. Springer, Dordrecht, 133-151.

Pye, K., Tsoar, H., 2008. Aeolian sand and sand dunes. Springer Science & Business Media.

Resentini, A., Andò, S., Garzanti, E., 2018. Quantifying roundness of detrital minerals by image analysis: sediment transport, shape effects, and provenance implications. Journal of Sedimentary Research 88, 276–289.

Rittner, M., Vermeesch, P., Carter, A., Bird, A., Stevens, T., Garzanti, E., Andò, S., Vezzoli, G., Dutt, R., Xu, Z., Lu, H., 2016. The provenance of Taklamakan desert sand. Earth and Planetary Science Letters 437, 127-137.

Rogers, J.W., Ghuma, M.A., Nagy, R.M., Greenburg, J.K., Fullagar, P.D., 1978. Plutonism in Pan-African belts and the geologic evolution of northeastern Africa. Earth Planetary Science Letters 39, 109–117.

Salze, D., Belcourt, O., Harouna, M., 2018. The first stage in the formation of the uranium deposit of Arlit, Niger: Role of a new non-continental organic matter. Ore Geology Reviews 102, 604-617.

Sarnthein, M., 1978. Sand deserts during glacial maximum and climatic optimum. Nature 272, 43-46.

Schandelmeier, H., Darbyshire, D.P.F., Harms, U., Richter, A., 1988. The E Saharan craton: Evidence for pre-Pan-African crust in NE Africa W of the Nile. In: El-Gaby, S., Greiling, R.O. (eds.), The Pan-African belts of NE Africa and Adjacent areas. Friedrich Vieweg and Sohn, 69-94.

Selley, R.C., 1997. The sedimentary basins of northwest Africa: Stratigraphy and sedimentation. In: Selley, R.C. (ed.), Sedimentary Basins of the World 3, African Basins. Elsevier, Amsterdam, 3-16.

Shaw, A., Goudie, A.S., 2002. Geomorphological evidence for the extension of the Mega-Kalahari into south-central Angola. South African Geographical Journal 84, 182–194.

Sláma, J., Košler, J., Condon, D.J., Crowley, J.L., Gerdes, A., Hanchar, J.M., Horstwood, M.S., Morris, G.A., Nasdala, L., Norberg, N., Schaltegger, U., 2008. Plešovice zircon—a new natural reference material for U–Pb and Hf isotopic microanalysis. Chemical Geology 249, 1-35.

Smith, B.J., Wright, J.S., Whalley, W.B., 2002. Sources of non-glacial, loess-size quartz silt and the origins of “desert loess”. Earth-Science Reviews 59, 1-26.

Stanistreet, I.G., Stollhofen, H., 2002. Hoanib River flood deposits of Namib Desert interdunes as analogues for thin permeability barrier mudstone layers in aeolianite reservoirs. Sedimentology 49, 719–736.

Stern, R.J., 1985. The Najd fault system, Saudi Arabia and Egypt: A late Precambrian rift- related transform system? Tectonics 4, 497-511.

Stern, R.J., Kröner, A., Reischmann, T., Bender, R., Dawoud, A.S., 1994. Precambrian basement around Wadi Halfa: A new perspective on the evolution of the Central Saharan Ghost craton. Geologische Rundschau 83, 564-577.

Stevens, T., Carter, A., Watson, T.P., Vermeesch, P., Andò, S., Bird, A.F., Lu, H., Garzanti, E., Cottam, M.A., Sevastjanova, I., 2013. Genetic linkage between the Yellow River, the Mu Us desert and the Chinese Loess Plateau. Quaternary Science Reviews 78, 355-368.

Sutcliffe, J.V., Parks, Y.P., 1999. The Hydrology of the Nile. International Association of Hydrological Sciences, Special Publication 5, 179 p.

Suttner, L.J., Basu, A., Mack, G.H., 1981. Climate and the origin of quartz arenites. Journal of Sedimentary Petrology 51, 1235–1246.

Svendsen, J., Stollhofen, H., Krapf, C.B.E., Stanistreet, I.G., 2003. Mass and hyperconcentrated flowdeposits record dune damming and catastrophic breakthrough of ephemeral rivers, Skeleton Coast Erg, Namibia. Sedimentary Geology 160, 7–31.

Swap, R., Garstang, M., Greco, S., Talbot, R., Kållberg, P., 1992. Saharan dust in the Amazon Basin. Tellus B, 44(2), 133-149.

Swezey, C., 2001. Eolian sediment responses to late Quaternary climate changes: Temporal and spatial patterns in the Sahara. Palaeogeography, Palaeoclimatology, Palaeoecology 167, 119-155.

Swezey, C.S., 2009. Cenozoic stratigraphy of the Sahara, northern Africa. Journal of African Earth Sciences, 53, 89-121.

Tegen, I., Schepanski, K., Heinold, B., 2013. Comparing two years of Saharan dust source activation obtained by regional modelling and satellite observations. Atmospheric Chemistry and Physics 13(5), 2381–2390.

Telbisz, T., Keszler, O., 2018. DEM-based morphometry of large-scale sand dune patterns in the Grand Erg Oriental (Northern Sahara Desert, Africa). Arabian Journal of Geosciences 11, 382.

Thomas, D.S.G., Shaw, P.A., 2002. Late Quaternary environmental change in central southern Africa: new data, synthesis, issues and prospects. Quaternary Science Reviews 21, 783–797.

Thomas, D.S.G., O'Connor, P.W., Bateman, M.D., Shaw, P.A., Stokes, S., Nash, D.J., 2000. Dune activity as a record of late Quaternary aridity in the northern Kalahari: new evidence from northern Namibia interpreted in the context of regional arid and humid chronologies. Palaeogeography Palaeoclimatology Palaeoecology 156, 243–259.

Thomas, R.J., Chevallier, L.P., Gresse, P.G., Harmer, R.E., Eglington, B.M., Armstrong, R.A., De Beer, C.H., Martini, J.E.J., De Kock, G.S., Macey, P.H., Ingram, B.A., 2002. Precambrian evolution of the Sirwa window, Anti-Atlas orogen, Morocco. Precambrian Research 118, 1-57.

Thusu, B., Mansouri, A., 1995. Reassignment of the Upper Amal Formation to Triassic and its implications for exploration in southeast Sirte, Libya. First Symposium on Hydrocarbon Geology of North Africa, London, 28–30 November, Abstracts 48.

Vainer, S., Dor, Y.B., Matmon, A., 2018. Coupling cosmogenic nuclides and luminescence dating into a unified accumulation model of aeolian landforms age and dynamics: The case study of the Kalahari Erg. Quaternary Geochronology 48, 133-144.

Vermeesch, P., 2013. Multi-sample comparison of detrital age distributions. Chemical Geology 341, 140-146.

Vermeesch, P., 2018a. IsoplotR: A free and open toolbox for geochronology. Geoscience Frontiers 9, 1479-1493.

Vermeesch, P., 2018b. Dissimilarity measures in detrital geochronology. Earth-Science Reviews, 178, 310-321.Statistical models for point-counting data. Earth and Planetary Science Letters 501, 112-118.

Vermeesch, P., 2021. On the treatment of discordant detrital zircon U–Pb data. Geochronology Discussions, 1-19. doi.org/10.5194/gchron-2020-38.

Vermeesch, P., Garzanti, E., 2015. Making geological sense of 'Big Data' in sedimentary provenance analysis. Chemical Geology 409, 20-27.

Vermeesch, P., Resentini, A., Garzanti, E., 2016. An R package for statistical provenance analysis. Sedimentary Geology 336, 14-25.

Vermeesch, P., Rittner, M., Petrou, E., Omma, J., Mattinson, C., Garzanti, E., 2017. High throughput petrochronology and sedimentary provenance analysis by automated phase mapping and LAICPMS. Geochemistry, Geophysics, Geosystems 18, doi.org/10.1002/2017GC007109.

Villeneuve, M., 2008. Review of the orogenic belts on the western side of the West African craton: Tthe Bassarides, Rokelides and Mauritanides. Geological Society, London, Special Publications 297, 169-201.

Wang, Q., Spencer, C.J., Hamdidouche, R., Zhao, G., Evans, N.J., McDonald, B.J., 2020. Detrital zircon U–Pb–Hf data from Cambrian sandstones of the Ougarta Mountains Algeria: Implication for palaeoenvironment. Geological Journal 55(12), 7760-7774.

Warner, T.T., 2009. Desert Meteorology. Cambridge University Press, 620 p.

Wilson, I.G., 1971. Desert sandflow basins and a model for the development of ergs. Geographical Journal 137(2), 180-199.

Zhang, D., Narteau, C., Rozier, O., Du Pont, S.C., 2012. Morphology and dynamics of star dunes from numerical modelling. Nature Geoscience, 5(7), 463-467.

Zuffa, G.G., 1985. Optical analyses of arenites: influence of methodology on compositional results In: Zuffa, G.G. (ed.), Provenance of Arenites. Reidel, Dordrecht, NATO ASI Series 148, 165-189.

Figure 1 Click here to access/download;Figure;Figure 1 Sahara Ergs.jpg

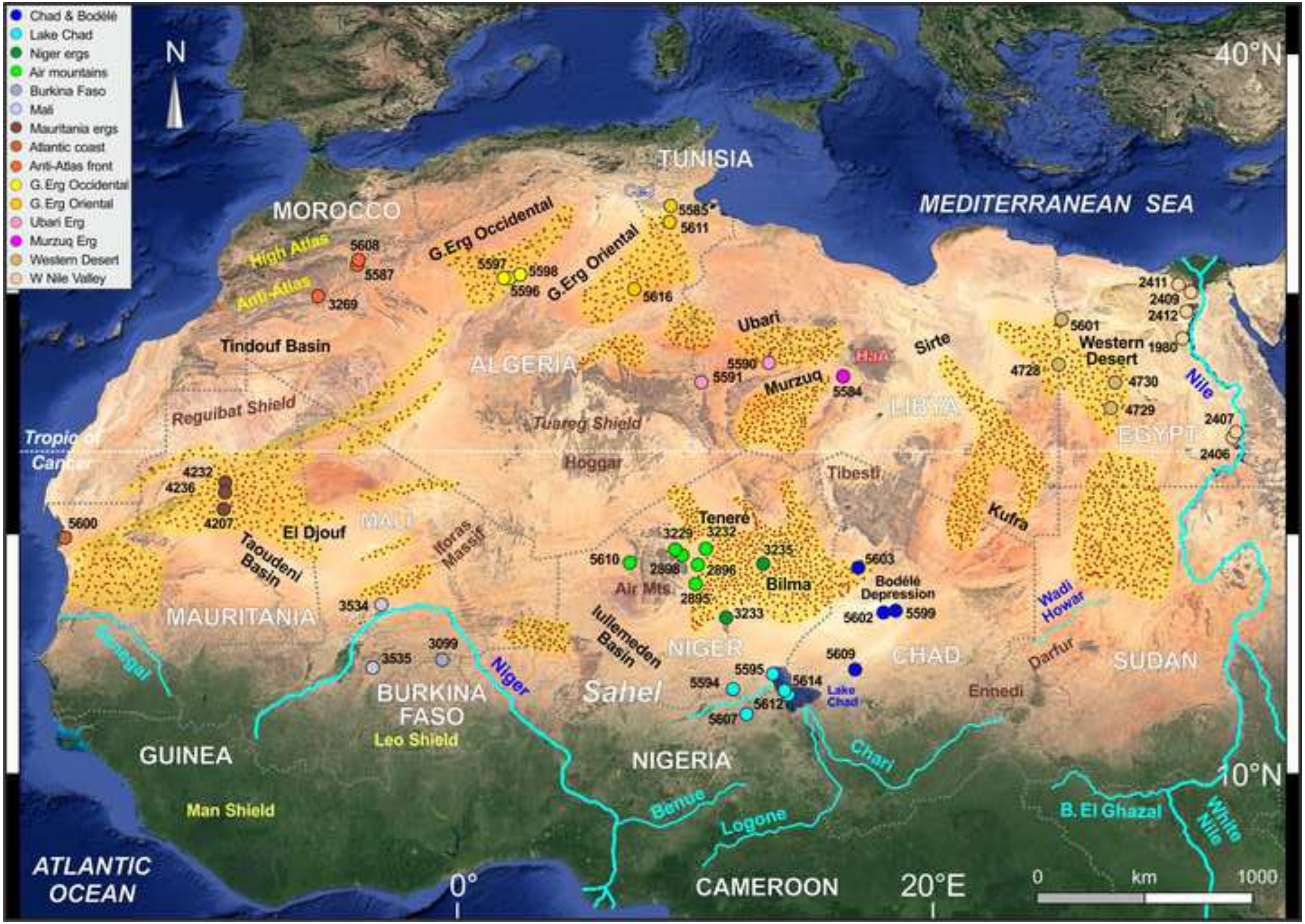

Figure 2

Click here to access/download;Figure;Figure 2 Sahara Wind.jpg

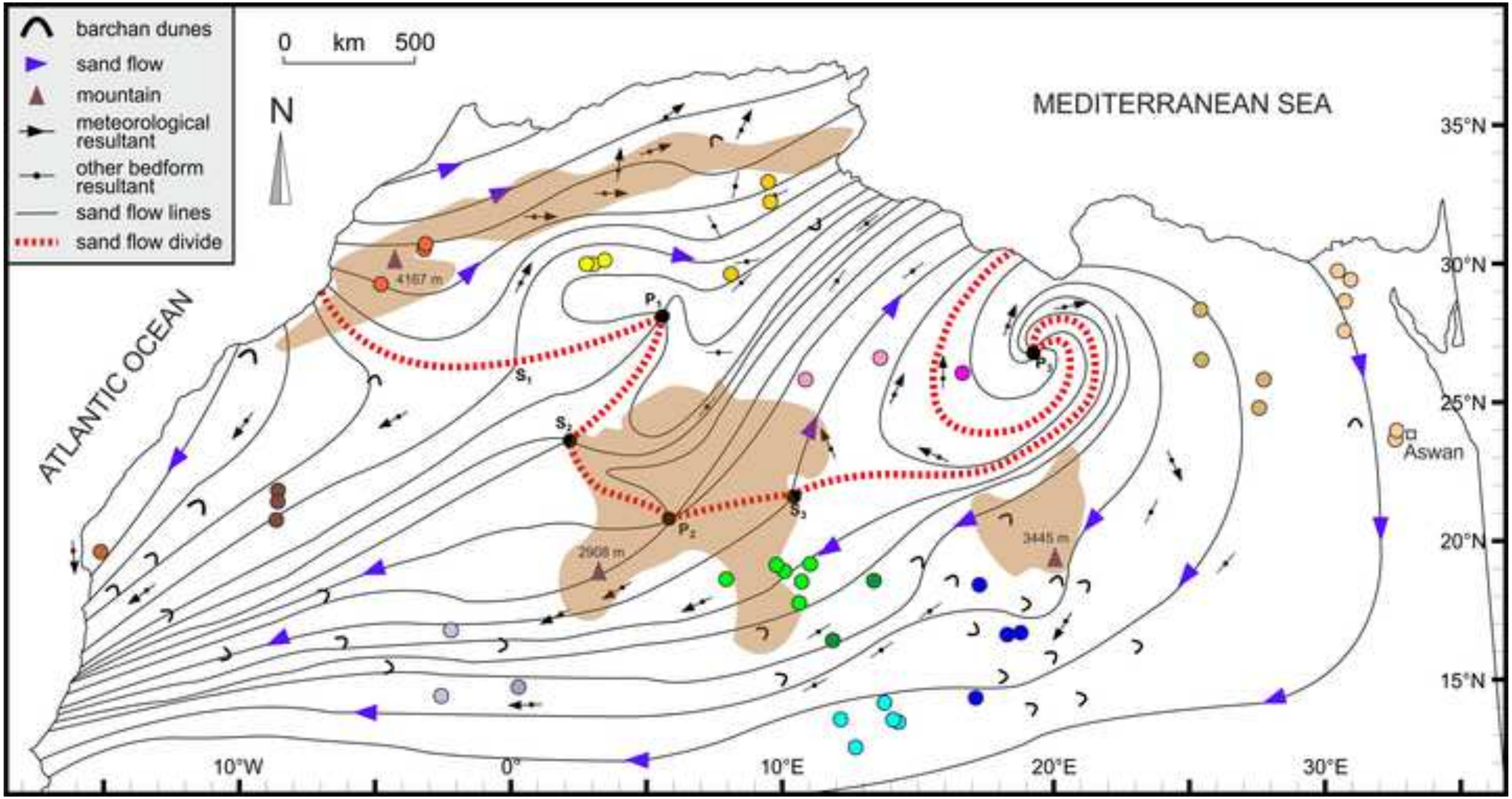

Figure 3

Click here to access/download;Figure;Figure 3 Sahara Geology.jpg

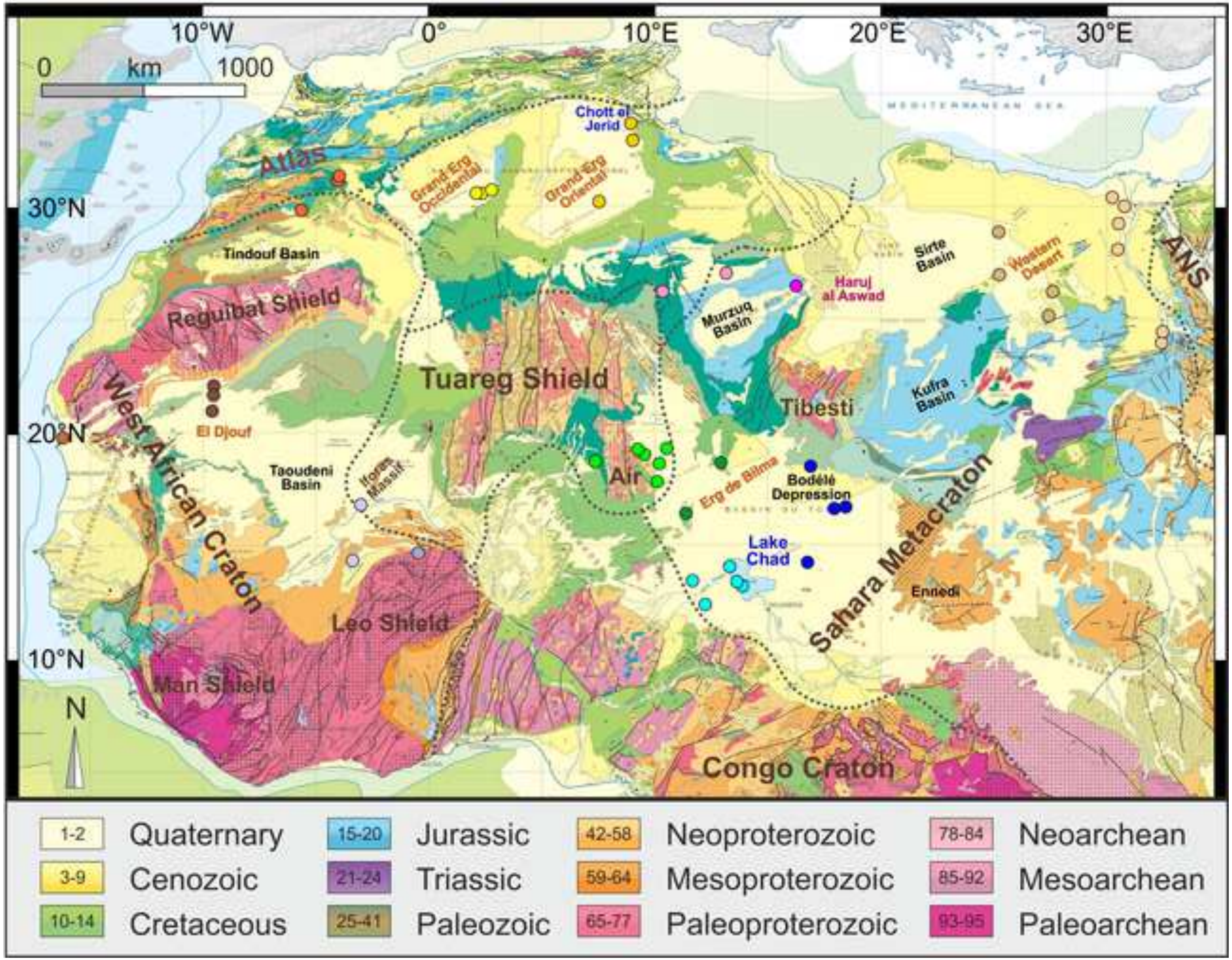

Figure 4

Click here to access/download;Figure;Figure 4 Sahara Photo PT.jpg

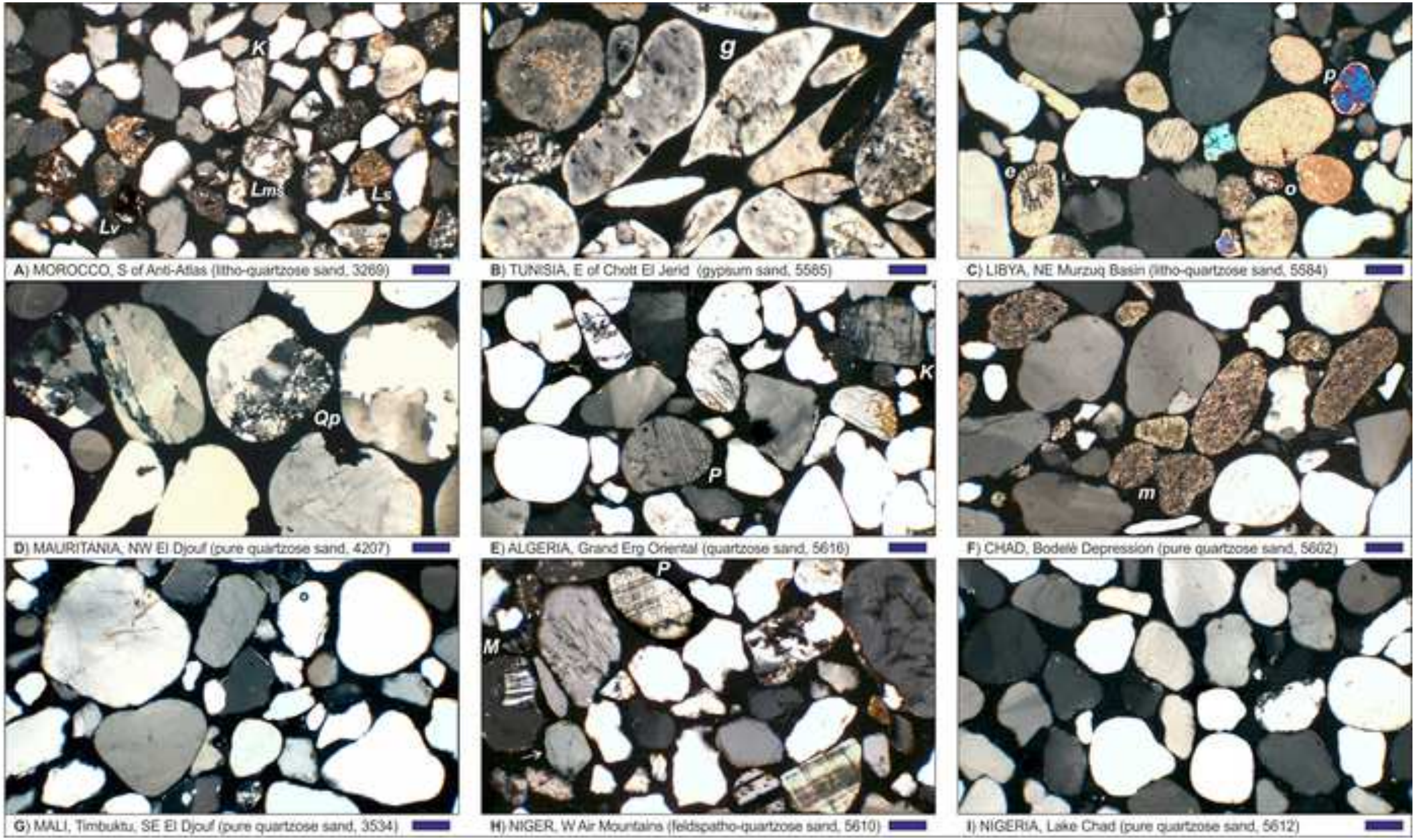

Figure 5

Click here to access/download;Figure;Figure 5 Sahara PT plots.jpg

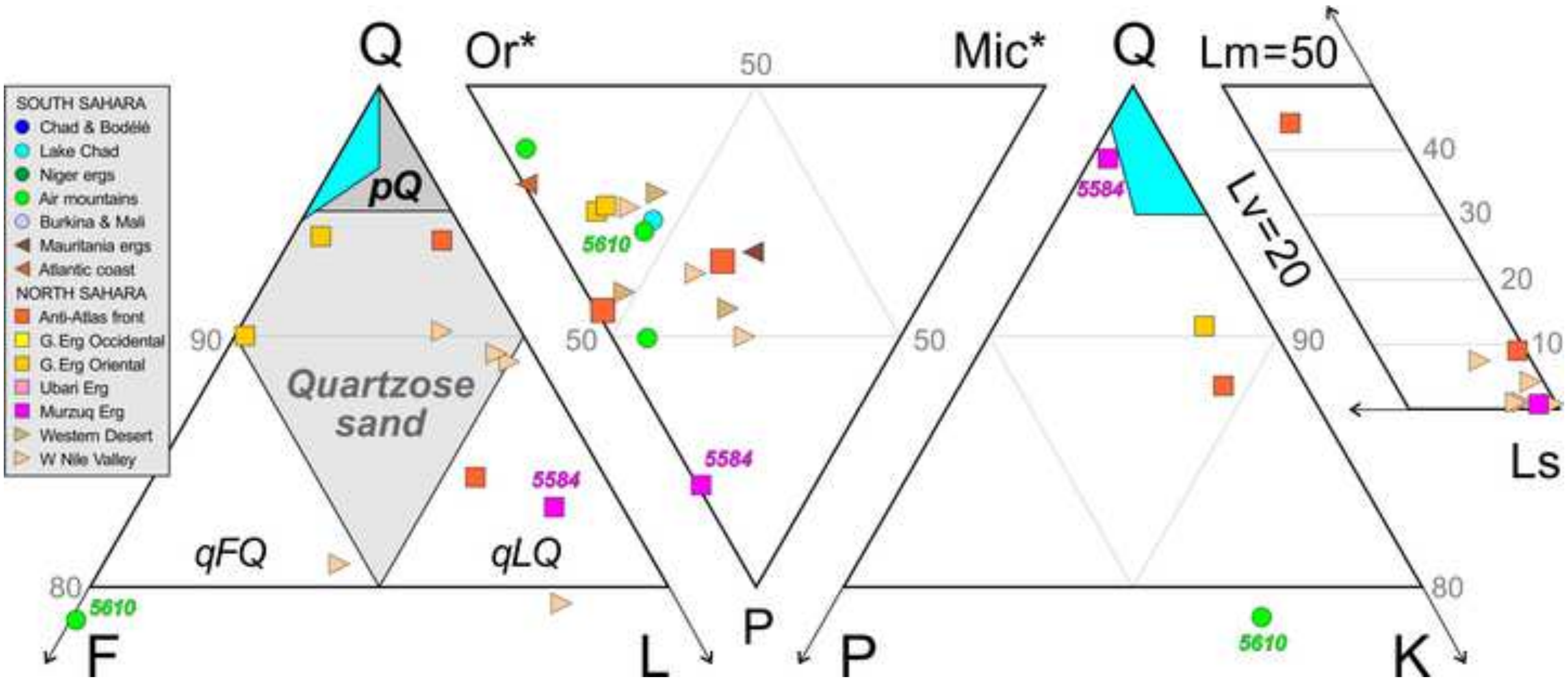

Figure 6

Click here to access/download;Figure;Figure 6 Sahara HM Biplot.jpg

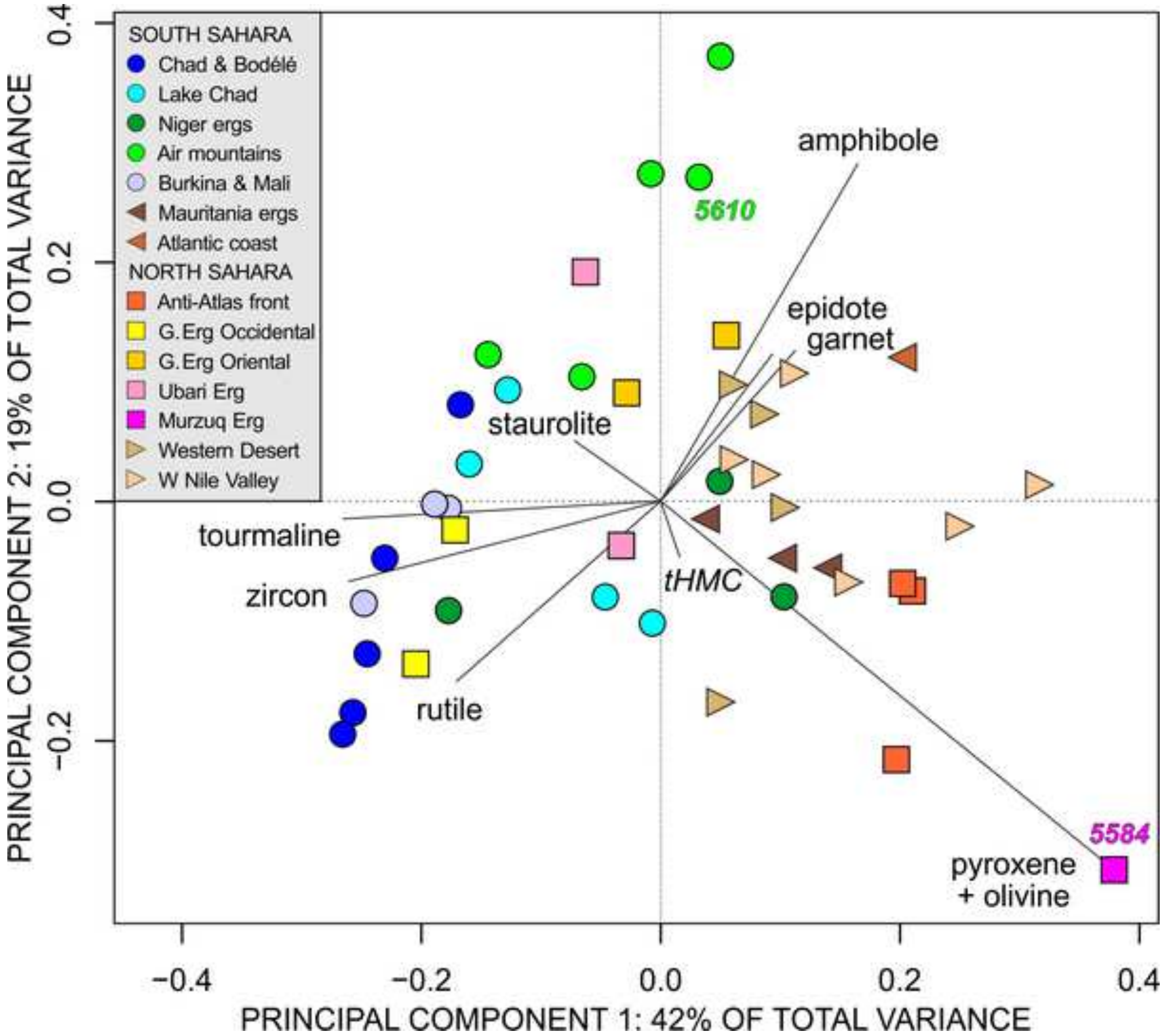

Figure 7

Click here to access/download;Figure;Figure 7 Sahara Zircon KDE.jpg

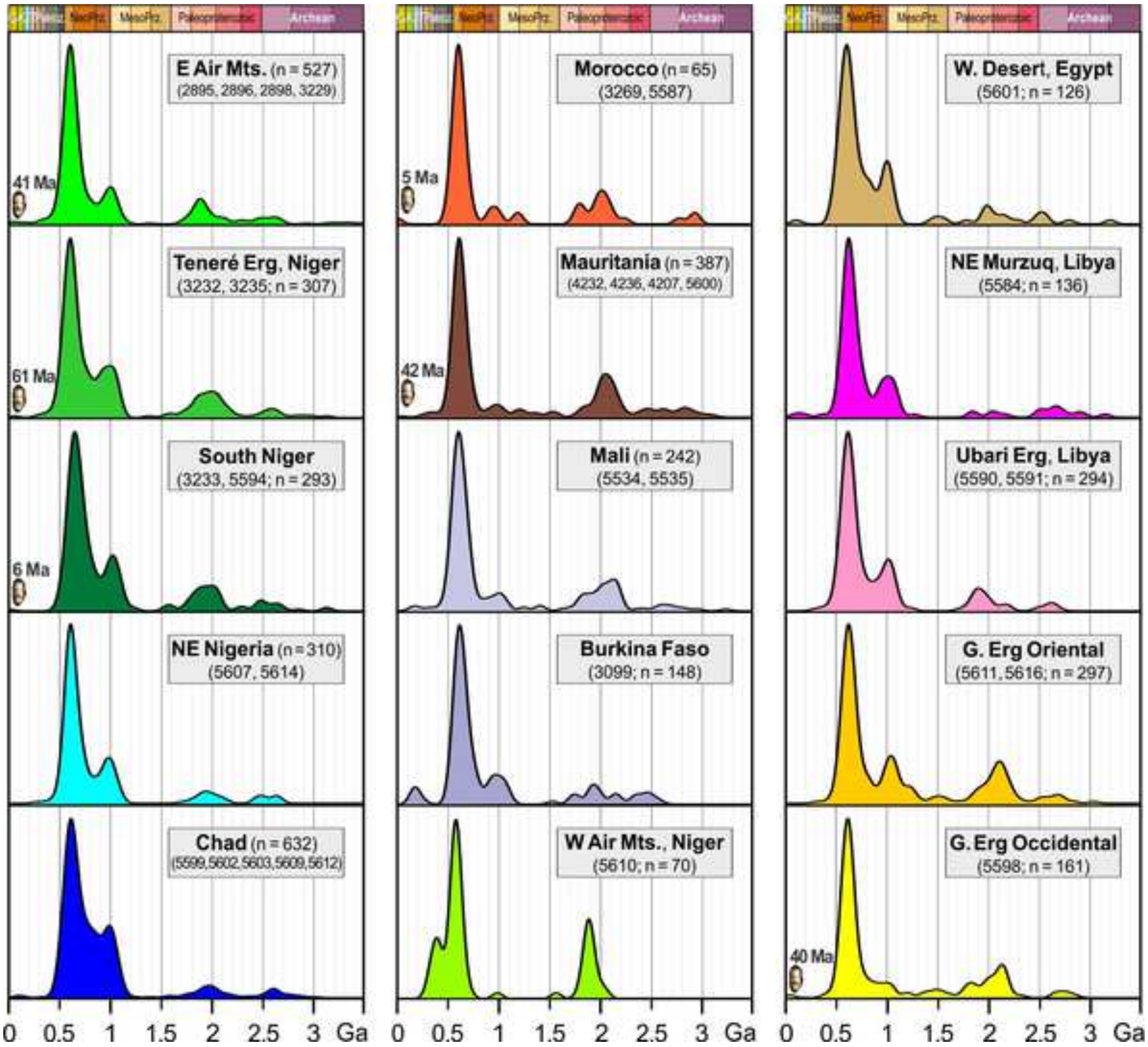

Figure 8 Click here to access/download;Figure;Figure 8 Sahara Statistics.jpg

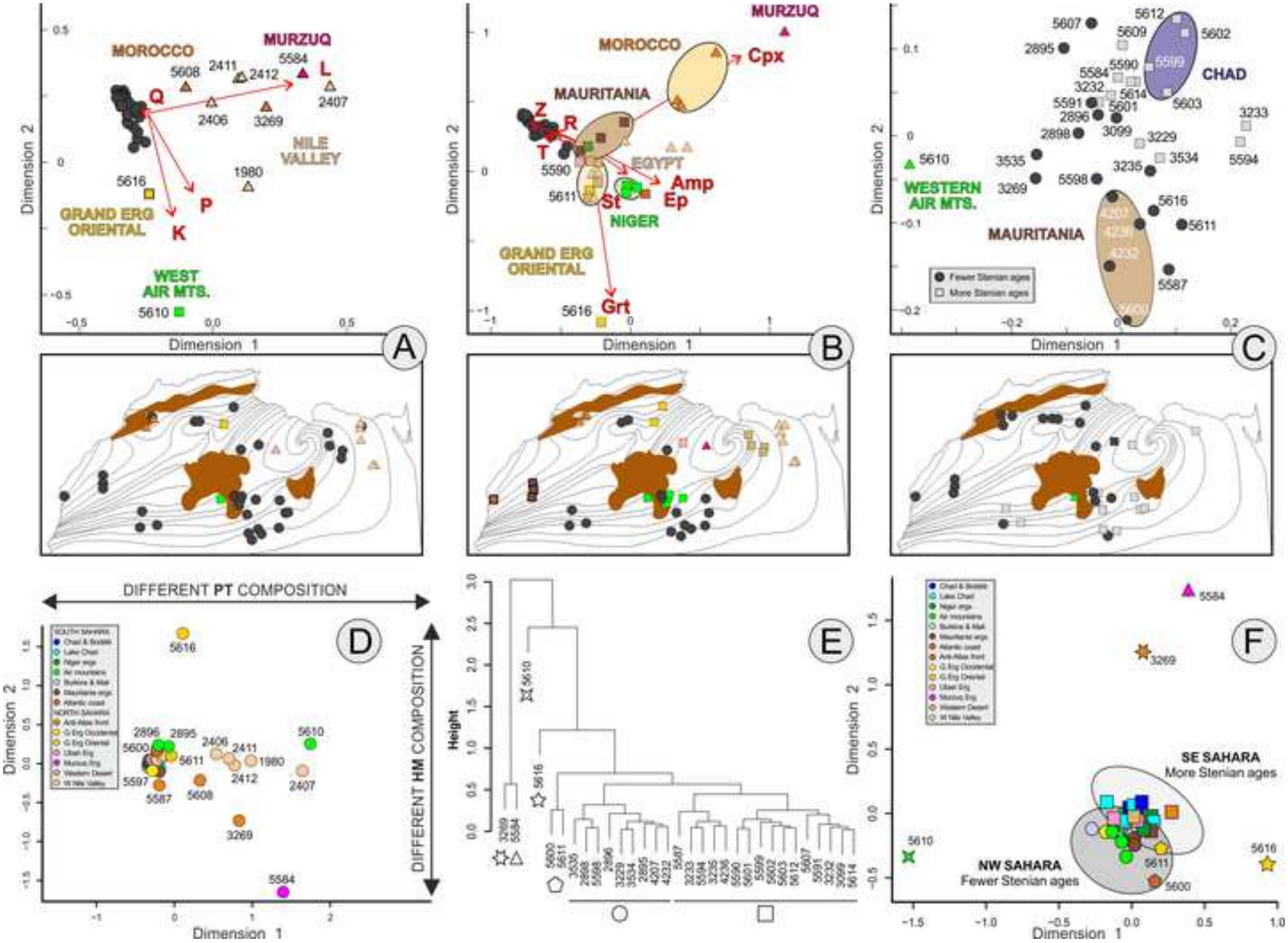

Figure 9

Click here to access/download;Figure;Figure 9 Sahara KDE Arabia Nilo.jpg

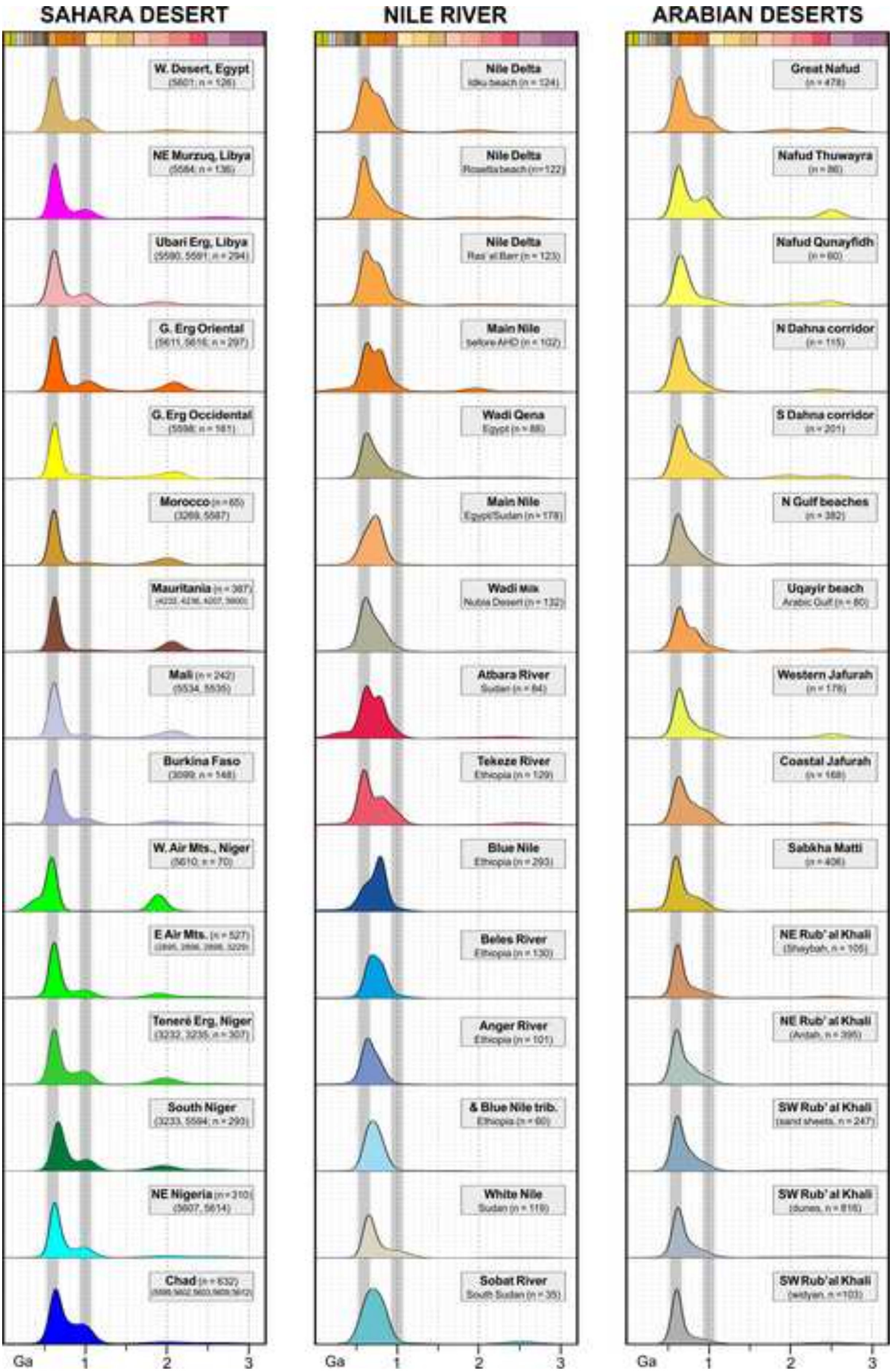

Figure 10 Click here to access/download;Figure;Figure 10 Sahara MDS.jpg

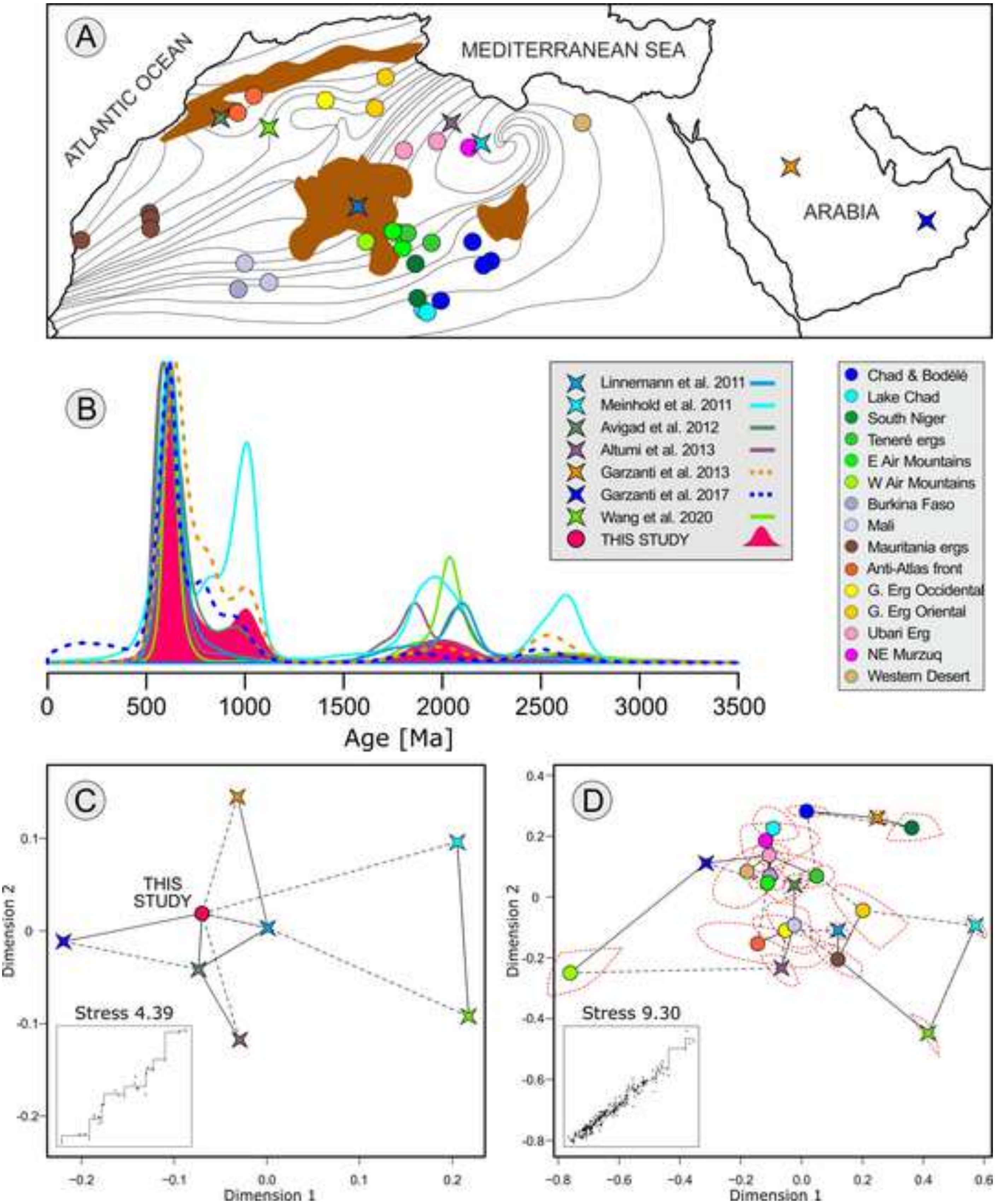

Table 1 Click here to access/download;Table;Table 1 Sahara PTHM Parameters.xlsx

| | n° | Q | F | Lv | Lc | Lsm | total | P/F | tHMC | ZTR | Ap | Ttn | Ep | P&P | Grt | St | Ky | Amp | Px | Ol | &tHM | total |
|---|---|---|---|---|---|---|---|---|---|---|---|---|---|---|---|---|---|---|---|---|---|---|
| CHAD & NIGERIA | | | | | | | | | | | | | | | | | | | | | | |
| Bodélé Depression | 4 | 99 | 0.8 | 0 | 0 | 0.1 | 100.0 | 0% | 0.1 | 81 | 1 | 2 | 8 | 0 | 1 | 1 | 0.3 | 3 | 1 | 0 | 1 | 100.0 |
| Lake Chad | 4 | 98 | 1 | 0 | 0 | 0.5 | 100.0 | 54% | 0.2 | 89 | 1 | 0.6 | 2 | 0 | 0.3 | 4 | 0.7 | 0.7 | 0 | 0 | 2 | 100.0 |
| NIGER, BURKINA, MALI | | | | | | | | | | | | | | | | | | | | | | |
| Southern Niger | 2 | 99 | 0.4 | 0 | 0 | 0.2 | 100.0 | 0% | 0.3 | 94 | 0.2 | 1 | 1 | 0 | 0.2 | 1 | 0 | 0.2 | 0 | 0 | 1 | 100.0 |
| Erg de Bilma | 2 | 98 | 1 | 0 | 0 | 0.5 | 100.0 | 58% | 0.2 | 60 | 0.5 | 1 | 13 | 0 | 7 | 2 | 0 | 6 | 9 | 0 | 0.2 | 100.0 |
| E Air Mountains | 2 | 99 | 0.7 | 0 | 0 | 0.3 | 100.0 | 0% | 0.1 | 69 | 0.5 | 0.5 | 7 | 0 | 0 | 10 | 0 | 11 | 0.2 | 0 | 2 | 100.0 |
| SE Air Mountains | 2 | 96 | 4 | 0 | 0 | 0.1 | 100.0 | 31% | 0.2 | 24 | 1 | 3 | 20 | 0 | 2 | 10 | 0 | 40 | 0 | 0 | 0.2 | 100.0 |
| W Air Mountains | 1 | 79 | 21 | 0 | 0 | 0 | 100.0 | 29% | 0.2 | 23 | 4 | 1 | 16 | 0 | 1 | 1 | 1 | 52 | 0 | 0 | 0.5 | 100.0 |
| Burkina Faso | 1 | 100 | 0 | 0 | 0 | 0.2 | 100.0 | n.d. | 0.2 | 77 | 0 | 0 | 20 | 0 | 0 | 2 | 0 | 0.5 | 0 | 0 | 0 | 100.0 |
| Mali | 2 | 100 | 0.2 | 0 | 0 | 0 | 100.0 | 50% | 0.1 | 91 | 0.2 | 0.5 | 3 | 0 | 0 | 3 | 1 | 0.5 | 0 | 0 | 0.5 | 100.0 |
| MAURITANIA | | | | | | | | | | | | | | | | | | | | | | |
| Coastal Mauritania | 1 | 97 | 3 | 0 | 0 | 0 | 100.0 | 33% | 1.2 | 16 | 0.5 | 0.5 | 35 | 0 | 6 | 1 | 0 | 35 | 4 | 0 | 2 | 100.0 |
| NW El Djouf | 3 | 99 | 0.8 | 0 | 0 | 0.3 | 100.0 | 10% | 0.1 | 50 | 1 | 0.4 | 21 | 0 | 4 | 4 | 0 | 5 | 13 | 0 | 1 | 100.0 |
| MOROCCO & ALGERIA | | | | | | | | | | | | | | | | | | | | | | |
| Anti-Atlas | 3 | 92 | 3 | 0.6 | 1 | 4 | 100.0 | 43% | 0.3 | 19 | 1 | 3 | 11 | 12 | 2 | 2 | 0 | 9 | 38 | 0 | 3 | 100.0 |
| Grand Erg Occidental | 2 | 99 | 0.6 | 0 | 0 | 0 | 100.0 | 33% | 0.1 | 93 | 0.2 | 0.4 | 5 | 0 | 2 | 0 | 0 | 0 | 0 | 0 | 0.2 | 100.0 |
| Grand Erg Oriental | 1 | 90 | 10 | 0 | 0 | 0.2 | 100.0 | 24% | 0.6 | 20 | 0 | 1 | 7 | 0 | 64 | 1 | 1 | 0 | 0 | 0 | 5 | 100.0 |
| TUNISIA & LIBYA | | | | | | | | | | | | | | | | | | | | | | |
| Grand Erg Oriental | 1 | 94 | 5 | 0 | 0.5 | 0.5 | 100.0 | 25% | 0.3 | 44 | 0.4 | 4 | 16 | 0 | 12 | 1 | 1 | 17 | 1 | 0 | 3 | 100.0 |
| Ubari Erg | 2 | 99 | 1 | 0 | 0 | 0 | 100.0 | 10% | 0.3 | 72 | 0 | 1 | 11 | 0 | 3 | 1 | 0 | 10 | 1 | 0 | 1 | 100.0 |
| NE Murzuq Erg | 1 | 83 | 2 | 0.2 | 14 | 0.7 | 100.0 | 80% | 1.1 | 2 | 0 | 0 | 2 | 0 | 0.5 | 0 | 0 | 0.5 | 56 | 38 | 1 | 100.0 |
| EGYPT | | | | | | | | | | | | | | | | | | | | | | |
| Western Desert | 4 | 97 | 3 | 0 | 0.3 | 0.2 | 100.0 | 39% | 0.1 | 44 | 1 | 2 | 23 | 0 | 11 | 5 | 1 | 6 | 5 | 0 | 1 | 100.0 |
| Aswan area | 2 | 85 | 3 | 0.3 | 9 | 2 | 100.0 | 44% | 1.5 | 11 | 0 | 0.2 | 30 | 0 | 2 | 3 | 0.7 | 29 | 23 | 0 | 1 | 100.0 |
| Nile Valley | 4 | 89 | 4 | 0.4 | 4 | 2 | 100.0 | 41% | 0.8 | 36 | 0.1 | 1 | 26 | 0 | 7 | 10 | 4 | 9 | 6 | 0 | 0.2 | 100.0 |

Table 2

Click here to access/download;Table;Table 2 Sahara Zircon Compilation.xlsx

| Study | Unit | Technique | concordant/ total ages | Age clusters | εHf(t) values |
|---|---|---|---|---|---|
| Linnemann et al. 2011 | Cambro-Ordovician Tassili Ouan Hoggar, Algeria | U-Pb (LA-ICP-MS) | 630/850 | 0.74-0.54 (61%), 2.2-2.0 (20%), 1.8-1.3 (7%), 0.98-0.75 (6%), 2.65-2.30 (3%) | |
| Meinhold et al. 2011 | Paleozoic-Mesozoic Murzuq, Libya | LA-SF-ICP-MS | 1257/1678 | 0.72-0.53 (39%), 1.06-0.92 (18%), 2.2-1.7 (16%), 2.75-2.50 (8%) | |
| Avigad et al. 2012 | Lower and Middle Cambrian, Morocco | LA-ICP-MS/Lu-Hf | 419/? | **Mid.Cambrian**: 0.63-0.54 (18%), 1.00-0.63 (61%), 1.2-1.0 (3%), 2.5-1.6 (16%) **Lower Cambrian**: 0.63-0.54 (71%), 1.00-0.63 (5%), 2.5-1.6 (23%) | **Neoproterozoic zircon**: **LC**: εHf(t) > 0; **MC**: εHf(t) < 0 |
| Altumi et al. 2013 | Cambrian Hasawnah Fm., Libya | LA-ICP-MS | 329/720 | 0.70-0.54 (60%), 2.4-1.6 (18%), 3.4-2.5 (5%) | |
| Wang et al. 2020 | Cambrian, Ougarta Mountains, Algeria | LA-ICP-MS/Lu-Hf | 449/536 | 0.80-0.56 (49%), 1.47-0.89 (2.4%), 3.4-1.6 (48%) | **0.6 Ga zircon**: +12/-25 (avg -1) **2.3-1.7 Ga zircon**: +6/-27 (avg -10) |
| Garzanti et al. 2013 | Northern Arabia sand seas | LA-ICP-MS | 1565/? | 1.0-0.5 (74%), 1.1-1.0 (8%), 2.0-1.8 (3%), 2.6-2.5 (3%) | |
| Garzanti et al. 2017 | Rub Al Khali, Saudi Arabia | LA-ICP-MS | 3909/5454 | 1.10-0.49 (85%), 2.15-1.74 (5%), 2.73-2.40 (5%) | |
| This study | Sahara Desert | LA-ICP-MS | 3996/5437 | 0.70-0.54 (51%), 1.1-0.9 (6%), 2.2-1.8 (11.7%) 2.70-2.47 (3%) | |